Groebke Blackburn Bienaymé-mediated multi-component synthesis of selective HDAC6 inhibitors with anti-inflammatory properties

Fabian B. Kraft,[a] Jana Enns,[b] Irina Honin,[a] Jonas Engelhardt,[b] Andrea Schöler,[c] Shannon T. Smith,[d] Jens Meiler,[c,d] Linda Schäker-Hübner,[a] Günther Weindl,[b] Finn K. Hansen[a]*

[a] Department of Pharmaceutical and Cell Biological Chemistry, Pharmaceutical Institute, University of Bonn, An der Immenburg 4, 53121 Bonn, Germany; [b] Department of Pharmacology and Toxicology, Pharmaceutical Institute, University of Bonn, Gerhard-Domagk-Str.3, 53121 Bonn, Germany; [c] Institute for Drug Discovery, Medicinal Faculty, University Leipzig, Brüderstraße 34, 04103 Leipzig, Germany;[d] Center for Structural Biology, Vanderbilt University, Nashville, TN 37240, USA; *Correspondence: finn.hansen@uni-bonn.de

Abstract

Histone deacetylases (HDACs) are a class of enzymes that cleave acyl groups from lysine residues of histone and non-histone proteins. There are 18 human HDAC isoforms with different cellular targets and functions. Among them, HDAC6 was found to be overexpressed in different types of cancer. However, when used in monotherapy, HDAC6 inhibition by selective inhibitors fails to show pronounced anti-cancer effects. The HDAC6 enzyme also addresses non-histone proteins like α-tubulin and cortactin, making it important for cell migration and angiogenesis. Recently, the NLRP3 inflammasome was identified as an important regulator of inflammation and immune responses and, importantly, HDAC6 is critically involved the activation of the inflammasome. We herein report the design, synthesis and biological evaluation of a library of selective HDAC6 inhibitors. Starting from the previously published crystal structure of **MAIP-032** in complex with CD2 of zHDAC6, we performed docking studies to evaluate additional possible interactions of the cap group with the L1-loop pocket. Based on the results we synthesized 13 novel HDAC6 inhibitors *via* the *Groebke-Blackburn-Bienaymé* three component reaction as the key step. Compounds **8k** (HDAC1 IC_{50}: 5.87 μM; HDAC6 IC_{50}: 0.024 μM; selectivity factor ($SF^{1/6}$): 245) and **8m** (HDAC1 IC_{50}: 3.07 μM; HDAC6 IC_{50}: 0.026 μM; $SF^{1/6}$: 118) emerged as the most potent and selective inhibitors of HDAC6 and outperformed the lead structure **MAIP-032** (HDAC1 IC_{50}: 2.20 μM; HDAC6 IC_{50}: 0.058 μM; $SF^{1/6}$: 38) both in terms of inhibitory potency and selectivity. Subsequent immunoblot analysis confirmed the high selectivity of **8k** and **8m** for HDAC6 in a cellular environment. While neither **8k** and **8m** nor the selectivity HDAC6 inhibitor tubastatin A showed antiproliferative effects in the U-87 MG glioblastoma cell line, compound **8m** attenuated cell migration significantly in wound healing assays in U-87 MG cells. Moreover, in macrophages compounds **8k** and **8m** demonstrated significant inhibition of LPS-induced *IL1B* mRNA expression and TNF release. These findings suggest that our imidazo[1,2-a]pyridine-capped HDAC6 inhibitors may serve as promising candidates for the development of drugs to effectively treat NLRP3 inflammasome-driven inflammatory diseases.

Keywords

Histone deacetylase, cancer, NLRP3 inflammasome, inflammation, HDAC6.

Abbreviations

CD: Catalytical domain; FDA: U.S. Food and Drug Administration; GBB: Groebke Blackburn Bienaymé; HDAC: Histone deacetylase; HSP90: Heat shock protein 90; IL1-b: Interleukin-1-beta; LDH: Lactate dehydrogenase; LPS: Lipopolysaccharaide; NLRP: Nucleotide-binding oligomerization domain; SEM: Standard error of the mean; SF: Selectivity factor; TLR: Toll like receptor; TNF: Tumor necrosis factor.

1 Introduction

Histone deacetylases (HDACs) are a class of enzymes, which remove acetyl groups from histone and non-histone proteins.[1] There are 18 human HDAC isoforms known, which can be divided into four classes, according to their structural features, homology, and cellular localization. Class I, II and IV HDACs possess a Zn^{2+} ion in their catalytic center. The remaining seven isoforms belong to the class III, the sirtuin family, which depend on the cofactor NAD^+ for their enzymatic activity.[2–4] HDACs have a direct influence on important cellular processes like cell proliferation[5] and migration.[6] The upregulation of HDAC enzymes has been implicated in a range of diseases, establishing them as valuable therapeutic targets.[7–9] Promising results have emerged from both preclinical and clinical studies demonstrating the efficacy of HDAC inhibition.[10–13] Notably, four non-selective HDAC inhibitors (HDACi) have obtained FDA approval for different hematological malignancies (Figure 1A).[9,14]

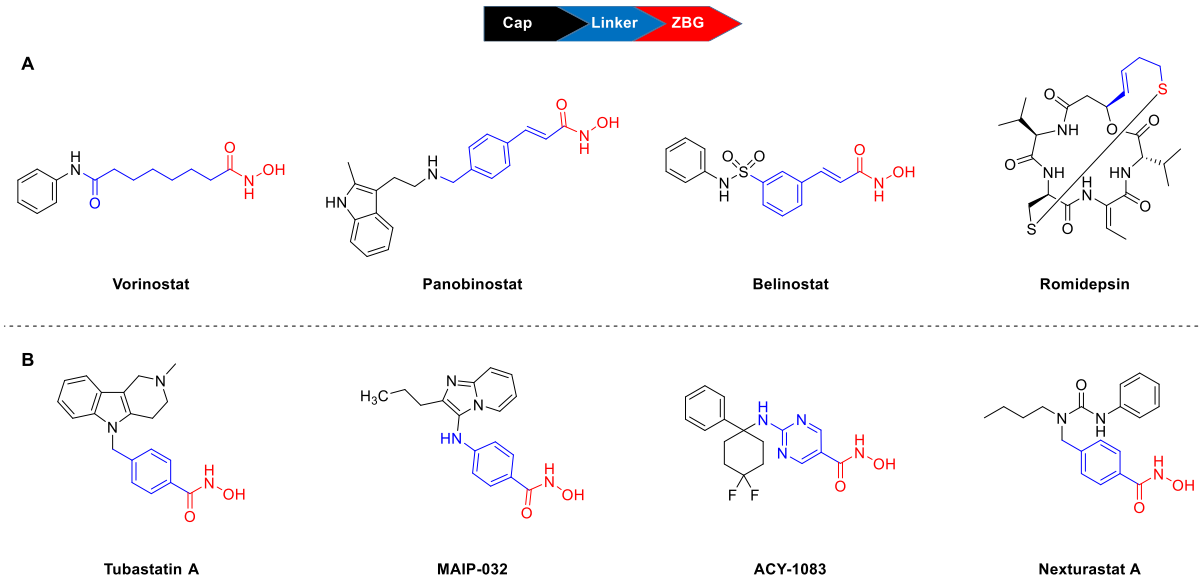

Figure 1. Selected HDACi including the pharmacophore model. Cap, linker, and ZBG are highlighted in black, blue, and red, respectively. **A**) FDA approved HDACi. Romidepsin binds via an *in situ* generated thiol. **B**) Selected HDAC6 preferential HDACi.[10]

Despite their success, those HDACi exhibit serious side effects, often leading to treatment interruption.[12,15] One way to circumvent unwanted side effects is the design of more selective inhibitors.[16] The HDAC6 enzyme, a member of class IIb, is mainly localized in the cytoplasm.[17] Unlike class I enzymes, HDAC6 addresses non-histone proteins like the cytoskeletal proteins α-tubulin, cortactin, and tau.[18–20] This makes HDAC6 a key player in various cellular processes, including tumor cell migration and angiogenesis[6] as well as in non-cancer diseases like fibrosis or alzheimer.[21] In addition, HDAC6 plays a crucial role in the refolding of misfolded proteins by activating Hsp90

and facilitating their targeted degradation through aggresome formation.[18] Despite being overexpressed in several cancer types, selective HDAC6 inhibition fails to show anti-cancer properties when used in monotherapy[22] and HDAC6 knock-out mice produce a viable phenotype.[23,24] This indicates a possible use of HDAC6 inhibitors beyond of oncology. Recently, HDAC6 has also been connected with the activation of the NLRP3 inflammasome. By acting as a dynein adaptor for microtubule transport, HDAC6 is crucial for inflammasome formation in mice, making it a potential therapeutic target for NLRP3 driven inflammatory diseases.[25] The NLRP3 inflammasome is a cytoplasmic complex involved in innate immunity and inflammation.[26] When activated, NLRP3 triggers the generation and release of pro-inflammatory cytokines like interleukin (IL)-1β, which plays a significant role in the development of chronic inflammatory diseases, including gout, rheumatoid arthritis, and inflammatory bowel disease.[27] Consequently, inhibition of the NLRP3 inflammasome has become a target for anti-inflammatory therapy.[28,29] HDAC10, the closest paralog of HDAC6, is implicated in various cellular processes, including cell cycle regulation and apoptosis, and is primarily acting as polyamine deacetylase.[30] Recent findings highlight that HDAC10 alleviates intracerebral hemorrhage (ICH)-induced injury by down-regulating the inflammatory response induced by NLRP3 inflammasomes through the protein tyrosine phosphatase, nonreceptor type 22 (PTPN22) pathway.[31] Additionally, according to a recent preprint, HDAC10 adversely modulates NLRP3 inflammasome activation by switching NLRP3 modification from acetylation to ubiquitination.[32]

HDAC6 is the largest isoform, composed of 1215 amino acids.[33] It consists of two catalytic domains (CD1 and CD2), which both exhibit deacetylase activity although with different substrate preferences. While the CD1 domain shows a high selectivity for substrates with C-terminal lysine residues,[34] the CD2 domain demonstrates a broader substrate range and is primarily responsible for the biological activity of HDAC6 inhibitors.[35] HDAC6 possesses unique structural features at the entrance to its catalytic pocket. Compared to other isoforms, these differences arise from the presence of two rigid loops. The L1-loop is primarily characterized by four amino acids (H463, P464, F583, and L712) that create a wide pocket, which can be engaged by HDACi with large, hydrophobic cap-groups. The L2-loop holds a "gatekeeper"–serine residue (S531), which is exclusive to the HDAC6 enzyme. Interactions with this residue are contributing to HDAC6 selectivity.[36] We recently reported the design and biological evaluation of imidazo[1,2-a]pyridine-capped HDAC6 preferential inhibitors.[37] Compound **MAIP-032** (Figure 1) showed the highest preference for HDAC6 over HDAC1, with a selectivity factor (SF) of 38. A crystal structure of HDAC6 CD2 domain from *Danio rerio* complexed with **MAIP-032** (PDB code 6CGP)[37] was obtained and revealed important interaction with the enzyme. Briefly, the Zn^{2+}-ion is complexed by the hydroxamic acid in a monodentate binding mode, while the bridging secondary amino-group forms a hydrogen bond with the aforementioned gatekeeper S531. Interestingly, the propyl side chain is oriented to the L1-loop, while the

heteroaromatic cap-group is oriented away from it. This stands in contrast to other, sterically demanding HDAC6 inhibitors, where the (hetero)aromatic cap-groups point towards the L1-pocket.[36] This distinctive binding mode forms a promising foundation for further optimization of **MAIP-032**.

While **MAIP-032** displayed promising inhibitory activity against HDAC6, its selectivity was only 38-fold over HDAC1. Given that HDAC1 is the primary contributor to the cytotoxic effects of HDAC inhibitors (HDACi), this limited selectivity falls short for advancing this compound as a viable treatment for non-oncological conditions, such as inflammation. Thus, the aim of this study was to perform a structure guided optimization campaign to develop highly selective HDAC6 inhibitors based on the imidazo[1,2-a]pyridine scaffold. In this work, we report the design, synthesis, and biological evaluation of the second generation of imidazo[1,2-a]pyridine-capped HDAC6 inhibitors.

2 Results and discussion

2.1 Docking studies

Based on the crystal structure of the HDAC6 CD2 domain in complex with **MAIP-032**, we hypothesized that modifications of the alkyl side chain can lead to enhanced interactions with the L1-loop and consequently to improved HDAC6 inhibitory activities. We first performed docking studies using *RosettaLigand* to investigate the scope of possible side chain lengths. Exemplary models for compounds **8a**, **8f**, and **8k** (for compound numbering see Table 1) are depicted in Figure 2 (for further information, see Supporting Information). All compounds showed a monodentate zinc-binding mode and a hydrogen bond interaction with the gatekeeper S531 as it was already observed for **MAIP-032**.[37] The methyl group of compound **8a** is slightly pointing away from the L1-loop indicating that the shortened side chain can lead to more flexibility in the cap orientation of the inhibitor. The longer pentyl side chain of compound **8f** seems to clash with the amino acids H500 and P501 of the L1-loop. The introduction of a fluorine atom in the linker in compound **8k** did not lead to any noteworthy changes compared to **MAIP-032**. However, it has recently been well elucidated that a fluorine atom in *meta*-position to the hydroxamic acid can increase the binding affinity due to the pi-pi interactions of the linker and additional interactions between the fluorine and the gatekeeper S531.[38]

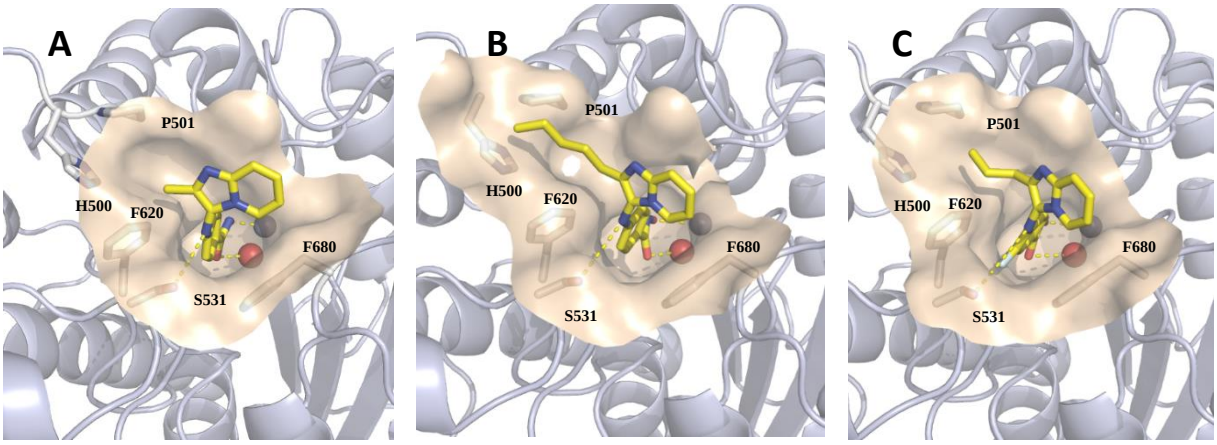

Figure 2. Docking pose of **8a** (**A**), **8f** (**B**), and **8k** (**C**) in the CD2 of *danio rerio* HDAC6 (PDB: 6CGP).[37] Ligands are colored yellow, the catalytic Zn^{2+}-ion and water molecule are shown as a gray and red sphere, respectively. Polar interactions are represented by dashed, yellow lines.

2.2 Design and synthesis

The target compounds were synthesized by a four-step procedure, with a *Groebke-Blackburn-Bienaymé* (GBB)[39] three component reaction as the key step to form the imidazo[1,2-a]pyridine core (Scheme 1). The synthesis required commercially available aldehydes and amidine components as well as isocyanides. The isocyanides were synthesized from their respective anilines in two steps. Initially, the anilines were formylated with formic acid in ethyl acetate to give the formamides **1**-**3** in 94% to quantitative yields. Next, they were dehydrated with phenyl phosphordichloridate to generate the individual isocyanides. The GBB reaction was performed either by addition of acetic acid with microwave assistance or with scandium(III) triflate as a catalyst at room temperature. In the final step, the hydroxamic acids **8a-m** were prepared *via* hydroxylaminolysis of the esters **7a-m**.

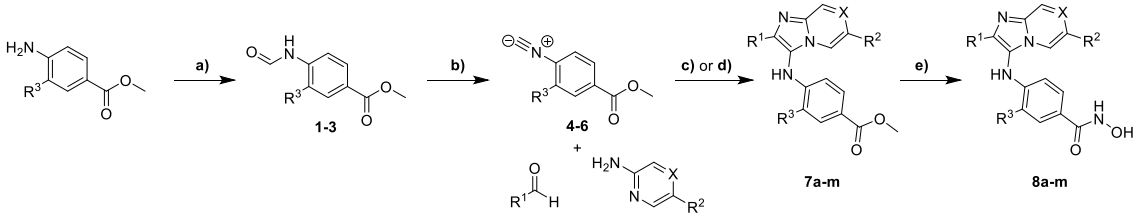

Scheme 1. Synthesis of imidazo[1,2-a]pyridine-capped HDAC inhibitors. **a)** CHOOH (20.0 eq), ethyl acetate, rt, 3 d; 94% - quant.; **b)** $PhOPOCl_2$ (1.20 eq.), NEt_3 (3.00 eq.), CH_2Cl_2, 0 °C to rt, 90 min, 61-94%; **c)** AcOH (2.00 eq.), MeOH, MW (110 W), 85 °C, 3 h, 27-84%; **d)** $Sc(OTf)_3$ (5 mol-%), MeOH/CH_2Cl_2 1/1 (*v*/*v*), rt, 3 d, 62%; **e)** NH_2OH_2 (50% in H_2O, 30.0 eq.), NaOH (10.0 eq.), MeOH/CH_2Cl_2 1/2 (*v*/*v*), 0 °C to rt, 90 min, 21 -92%.

All final compounds were characterized by ^{1}H-, ^{13}C-NMR spectroscopy as well as HRMS and HPLC analysis. The measured NMR spectra were in agreement with the expected values and all test compounds showed > 95% purity. Furthermore, in case of the fluorinated derivatives **8g**, **8k**, and **8m**, ^{19}F-NMR spectra clearly confirmed successful fluorination. The NMR spectra and HPLC chromatograms are provided in the Supporting Information.

2.3 Inhibitory activity against human HDAC isoforms

First, all synthesized hydroxamic acids were evaluated in biochemical HDAC inhibition assays for their inhibitory activity against human HDAC1 and HDAC6 isoforms using ZMAL as substrate.[40] The results are summarized in Table 1.

Table 1. Inhibitory activities of synthesized hydroxamic acids **8a-m**, **MAIP-032**, tubastatin A, and vorinostat against human HDAC1 and 6 isoforms.

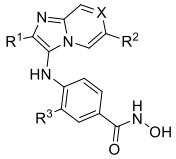

entry	R^1	R^2	R^3	HDAC1 IC_{50} [µM]	HDAC6 IC_{50} [µM]	SF[a]
8a (X = CH)	Methyl	H	H	2.746 ± 0.254	0.046 ± 0.004	60
8b (X = CH)	Ethyl	H	H	2.903 ± 0.191	0.075 ± 0.0004	39
8c (X = CH)	Isobutyl	H	H	3.705 ± 0.081	0.099 ± 0.005	37
8d (X = CH)	Cyclopropyl	H	H	2.515 ± 0.196	0.106 ± 0.016	24
8e (X = CH)	Butyl	H	H	3.294 ± 0.133	0.120 ± 0.001	27
8f (X = CH)	Pentyl	H	H	1.154 ± 0.071	0.081 ± 0.008	14
8g (X = CH)	$CH_2CH_2CF_3$	H	H	2.837 ± 0.049	0.230 ± 0.023	12
8h (X = CH)	Propyl	Methyl	H	2.554 ± 0.166	0.093 ± 0.003	27
8i (X = CH)	Propyl	Ethyl	H	1.356 ± 0.011	0.082 ± 0.017	16
8j (X = N)	Propyl	H	H	2.999 ± 0.393	0.115 ± 0.018	26
8k (X = CH)	Propyl	H	F	5.872 ± 0.981	0.024 ± 0.003	245
8l (X = CH)	Propyl	H	Methyl	19.77 ± 0.948	0.589 ± 0.001	34
8m (X = CH)	Methyl	H	F	3.068 ± 0.144	0.026 ± 0.001	118
Vorinostat	/	/	/	0.089 ± 0.001	0.029 ± 0.002	3
MAIP-032[b] (X = CH)	Propyl	H	H	2.20 ± 0.33	0.058 ± 0.012	38
Tubastatin A[b]	/	/	/	2.49 ± 0.14	0.014 ± 0.001	178

[a] Selectivity factor (SF) = IC_{50} (HDAC1)/ IC_{50} (HDAC6); [b] Data taken from *Mackwitz et al.*[37]

We started the structural modification on the side chain R^1 of the cap group to improve the interaction with the L1-loop. As expected from our docking studies, shorter alkyl chains showed a better inhibitory activity and selectivity profile for HDAC6. Inhibitor **8a** (IC_{50} (HDAC6) = 0.046 µM), with the shortest side chain, showed a comparable HDAC6 activity to the reference inhibitor **MAIP-032** (IC_{50} (HDAC6) = 0.058 µM) but also a lower HDAC1 inhibition, thus resulting in an increased selectivity. Prolonging the chain further, the HDAC6 inhibitory activity declined up to 0.120 µM (SF: 27) for the butyl group (**8e**). Remarkably, the compound **8f**, with a pentyl side chain, exhibited an increased inhibitory activity against both isoforms. In contrast to our expectations, the 3,3,3-trifluoropropyl derivative (**8g**) displayed nearly fourfold lower inhibition of HDAC6 and threefold lower selectivity compared to **MAIP-032**. This suggests that the additional, hypothesized interactions with the L1-pocket, might not be feasible in this case. Similarly, the introduction of branched (**8c**) or short, cyclic (**8d**) side chain both resulted in a decreased HDAC6 inhibitory activity. Next, we aimed to optimize the heterocyclic cap group. To achieve this, we introduced alkyl chains at the 6-position (**8h** and **8i**), which failed to improve HDAC6 inhibition, but increased HDAC1 inhibition. Furthermore, the pyrazine-based inhibitor **8j** exhibited an overall lower activity compared to **MAIP-032**. Next, we modified the linker to improve the hydrogen bond interaction of the bridging secondary amino group with S531. Initially, the introduction of a methyl group at the 3-position (**8l**) on the linker substantially attenuated the inhibition on both isoforms. However, when a fluorine atom was introduced (**8k**), we observed a twofold increase in HDAC6 activity and remarkable sixfold improvement in selectivity over HDAC1 (IC_{50} (HDAC6) = 0.024 µM; SF: 245). Notably, **8k** outperformed the selectivity profile of the gold standard selective HDAC6 inhibitor tubastatin A (SF: 178). Encouraged by these findings, we proceeded to combine the methyl side chain with the fluorinated linker, resulting in the synthesis of inhibitor **8m**. Interestingly, compound **8m** (IC_{50} (HDAC6) = 0.026 nM; SF: 118) showed comparable HDAC6 inhibition to **8k**, but displayed also better HDAC1 activity, which consequently led to a lower selectivity. The most important structure-activity relationships from our previous work[37] and this series of compounds are summarized in Figure 3.

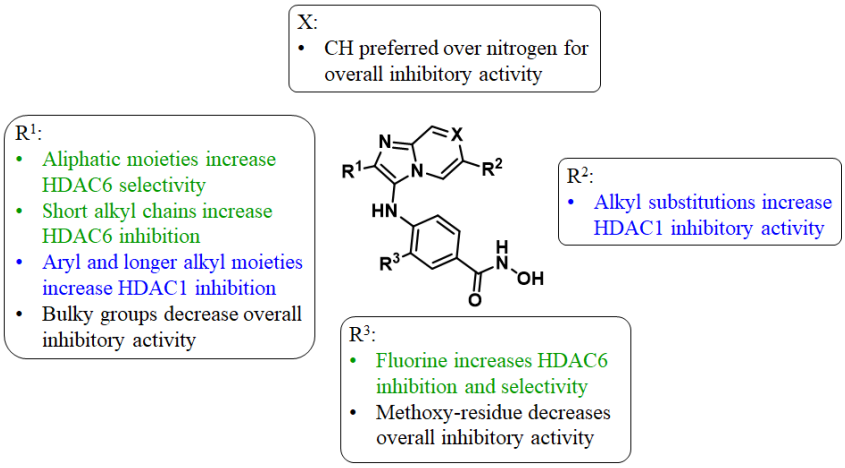

Figure 3. Structure-activity relationships of imidazo[1,2-a]pyridine based HDACi.

With the two most promising compound **8k** and **8m**, we continued to test their activity against further class I and isoforms (see Table 2). The inhibitor **8k** showed a very high selectivity of $SF^{2/6}$: 460 (HDAC2) and $SF^{3/6}$: 919 (HDAC3), which is 1.7- and 2.1-fold higher than in the case of **8m**. Finally, **8k** and **8m** were screened for their inhibitory activity against HDAC10, the closest paralog of HDAC6. Both compounds showed only moderate inhibition of HDAC10, further supporting that **8k** (HDAC10 IC_{50}: 1.11 µM) and **8m** (HDAC10 IC_{50}: 0.562 µM) are selective HDAC6 inhibitors.

Table 2. Extended isoform profiling of hit compounds **8k** and **8m** against human HDAC1,2,3 and HDAC6.

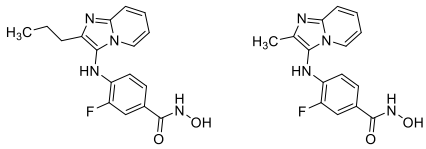

8k **8m**

entry	HDAC1 IC_{50} [µM]	HDAC2 IC_{50} [µM]	HDAC3 IC_{50} [µM]	HDAC6 IC_{50} [µM]	HDAC10 IC_{50} [µM]	$SF^{1/6}$	$SF^{2/6}$	$SF^{3/6}$	$SF^{10/6}$
8k	5.872 ± 0.981	11.04 ± 0.594	22.06 ± 3.019	0.024 ± 0.003	1.11 ± 0.07	245	460	919	46
8m	3.068 ± 0.144	6.858 ± 0.238	11.03 ± 1.531	0.026 ± 0.001	0.562 ± 0.046	118	264	424	22
Vorinostat	0.089 ± 0.001	0.202 ± 0.001	0.128 ± 0.004	0.029 ± 0.002	n.d.	3	7	4	n.d.
Quisinostat	n.d.	n.d.	n.d.	n.d.	0.005 ± 0.0004	n.d.	n.d.	n.d.	n.d.

n.d.: not determined

2.4 Cellular HDAC inhibition and anticancer effects in the U-87 MG glioblastoma cell line

Motivated by the potent and selective inhibition of HDAC6 in biochemical HDAC assays, we decided to investigate the properties of the hit compounds **8k** and **8m** in more detail. To assess the cellular target engagement of compounds **8k** and **8m** for HDAC6, we treated the glioblastoma cell line U-87 MG with **8k**, **8m**, tubastatin A, and vorinostat for 24 hours. The following western blot analysis showed α-tubulin hyperacetylation (Ac-α-tubulin), a well-known indicator of HDAC6 inhibition (Figure 4) in the case of **8k**, **8m**, tubastatin A, as well as vorinostat. In contrast, the acetylation status of histone H3 (Ac-H3) remained unaffected following the treatment with **8k**, **8m**, and tubastatin A while the unselective HDAC inhibitor vorinostat induced significant hyperacetylation of histone H3. Since Ac-H3 serves as a marker for class I HDAC inhibition, these results confirm the HDAC6 selectivity of **8k** and **8m** in a cellular environment.

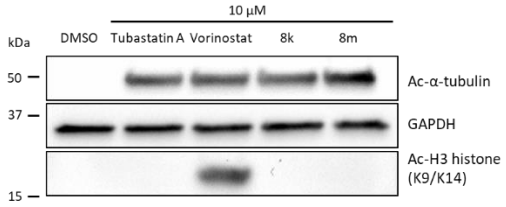

Figure 4. Representative immunoblot analysis of acetylated α-tubulin and histone H3. U-87 MG cells were incubated for 24 h with 10 µM of tubastatin A, vorinostat, **8k**, and **8m**. Afterwards, cell lysates were immunoblotted with anti-acetyl-α-tubulin and anti-acetyl-histone H3 (K9/K14) antibodies. GAPDH was used as a loading control.

Next, we evaluated the anticancer properties of **8k** and **8m**. To this end, we analyzed the antiproliferative activity of **8k** and **8m** in a MTT assay in the glioblastoma cell line U-87 MG using tubastatin A and vorinostat as control compounds. The results are summarized in Table 3. As expected, the HDAC6 selective inhibitors **8k**, **8m**, and tubastatin A had only minor effects on the cell viability with IC_{50} values ranging from 16.1 to 24.7 µM, while vorinostat demonstrated more potent antiproliferative activity (IC_{50} (U-87 MG) = 4.60 µM). This is in accordance with recent studies by us and others that indicate low single-agent cytotoxic properties of selective HDAC6 inhibitors.[22,41]

Table 3. Antiproliferative activity of **8k** and **8m** against the glioblastoma cell line U-87 MG. [a]

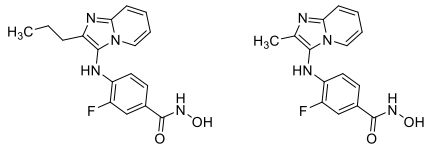

8k **8m**

entry	U-87 MG IC_{50} [µM]
8k	19.5 ± 3.26
8m	16.1 ± 1.54
Tubastatin A	24.7 ± 2.12
Vorinostat	4.60 ± 0.44

[a]Stated IC_{50} values were determined from the mean of at least three independent experiments in duplicates.

2.5 Wound healing assay in the U-87 MG cell line

HDAC6 plays a crucial role in cell migration by regulating processes such as microtubule dynamics, cytoskeletal remodeling, and cell signaling. The U-87 MG cell line has proven effective in prior research for investigating the anti-migratory properties of selective HDAC6 inhibitors.[42] We thus used this cell line to investigate the anti-migratory potential of tubastatin A, vorinostat, **8k**, and **8m** in wound healing assays. To this end, the cells were pretreated with 10 µM of the respective HDAC6i and cell migration was followed over 48 h and compared to the DMSO treated control cells. The results are presented in Figure 5. Tubastatin A, vorinostat, and **8k** had no significant effects on cell migration, while **8m** attenuated cell migration significantly.

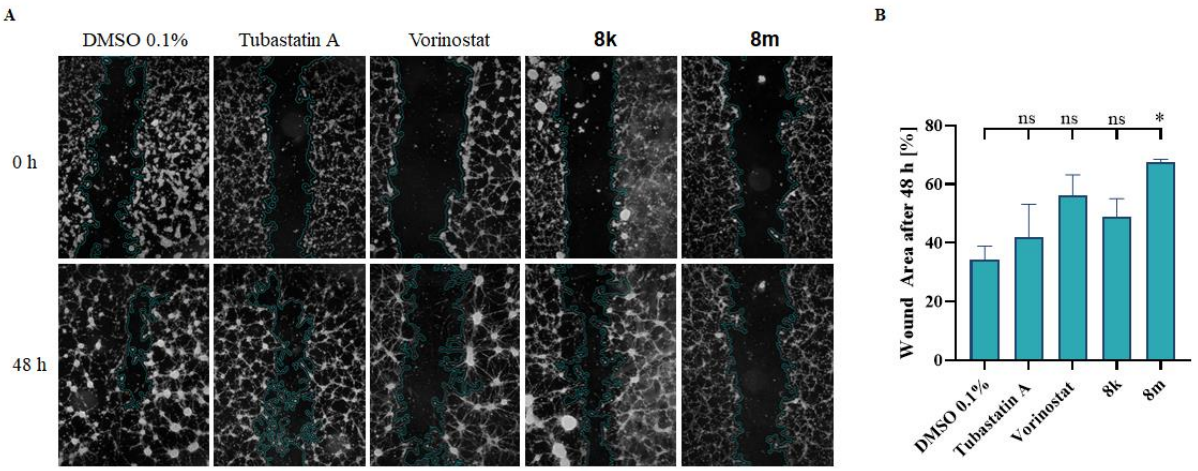

Figure 5. Wound healing assay in U-87 MG cells which were treated with selected HDACi (10 µM) or vehicle (0.1% DMSO). (A) Representative images taken immediately after scratching (0 h) and after 48 h. (B) Quantification of remaining wound area compared to the initial wound area. Mean + SEM, n = 3. Significances

were determined by one-way ANOVA followed by Dunnett's multiple comparisons test and are indicated by asterisks (ns = not significant; *P ≤ 0.05).

2.6 NLRP3-mediated IL1-β release

Although selective HDAC6 inhibitors hold great potential as anticancer agents when used in combination therapies e.g. with proteasome inhibitors, there is growing evidence that HDAC6 inhibitors may offer therapeutic benefits in various diseases beyond oncology. In addition to its involvement in various other cellular processes, HDAC6 has recently been implicated in NLRP3 inflammasome-related inflammatory responses.[25,43,44] Consequently, selective HDAC6 inhibitors present a promising new option for the treatment of diseases associated with the NLRP3 inflammasome. However, the underlying mechanisms are poorly understood and the mechanistic role of HDAC6 in NLRP3-mediated IL-1β release remains controversial. It has been reported that HDAC6 inhibitors have been reported to attenuate NLRP3-mediated inflammation,[44–46] however, other studies demonstrate that tubastatin A shows no effect on ATP-induced IL-1β release in mouse cells[47]. To determine effects of HDAC6 inhibition on NLPR3 inflammasome activation, lipopolysaccharide (LPS)-primed THP-1 macrophages were incubated with tubastatin A, **MAIP-032**, and the two most potent inhibitors **8k** and **8m** at concentrations ranging from 0.01 to 100 µM, followed by stimulation with ATP or nigericin. However, none of the HDAC6 inhibitors demonstrated a decrease in IL-1β release (Figure S1, Supporting Information). Consistent with our previous findings,[48] the NLRP3 inflammasome inhibitor MCC90 suppressed IL-1β release induced by nigericin, but it did not show inhibitory effects in the presence of ATP. Similar results were observed when LDH release was determined to monitor pyroptosis. This indicates that HDAC6 is dispensable for IL-1β release during NLRP3 inflammasome activation in human macrophages which confirms our recent findings.[49] Since studies have demonstrated that HDAC6 inhibitors suppress the activation of the NLRP3 inflammasome in mice,[25] we next used mouse J774A.1 macrophages. Tubastatin A and **8k** reduced nigericin- but not ATP-induced IL-1β release at 50 and 100 µM, respectively (Figure S2, Supporting Information). As expected, MCC950 completely blocked IL-1β release. Notably, in our experimental setting, J774.1 macrophages released 30-times higher IL-1β levels compared to previous studies using immortalized mouse bone marrow–derived macrophages.[25] This indicates, that HDAC6 inhibitors show only a weak inhibitory effect on NLRP3 inflammasome activation in mouse cells that release high levels of IL-1β.

Previously, we demonstrated that inhibition of HDAC6 by tubastatin A interferes with TLR signaling, which inhibits NLRP3-inflammasome mediated IL-1β release by human macrophages.[49] Thus, we tested whether HDAC6 inhibitors block the release of IL-1β by suppressing TLR-mediated priming in THP-1 macrophages.

Tubastatin A, as well as **MAIP-032**, **8k**, and **8m** significantly inhibited LPS-induced *IL1B* mRNA expression and TNF release at 10 µM (Figure 6A). In line with our previous observations,[49] vorinostat completely blocked TLR4-mediated responses, suggesting that inhibition of other HDACs contributes to this effect. We confirmed that vorinostat but not the selective HDAC6 inhibitors induced histone-H3 acetylation (Ac-H3) in THP-1 macrophages with **8k** and **8m** being highly selective (Figure 6B).

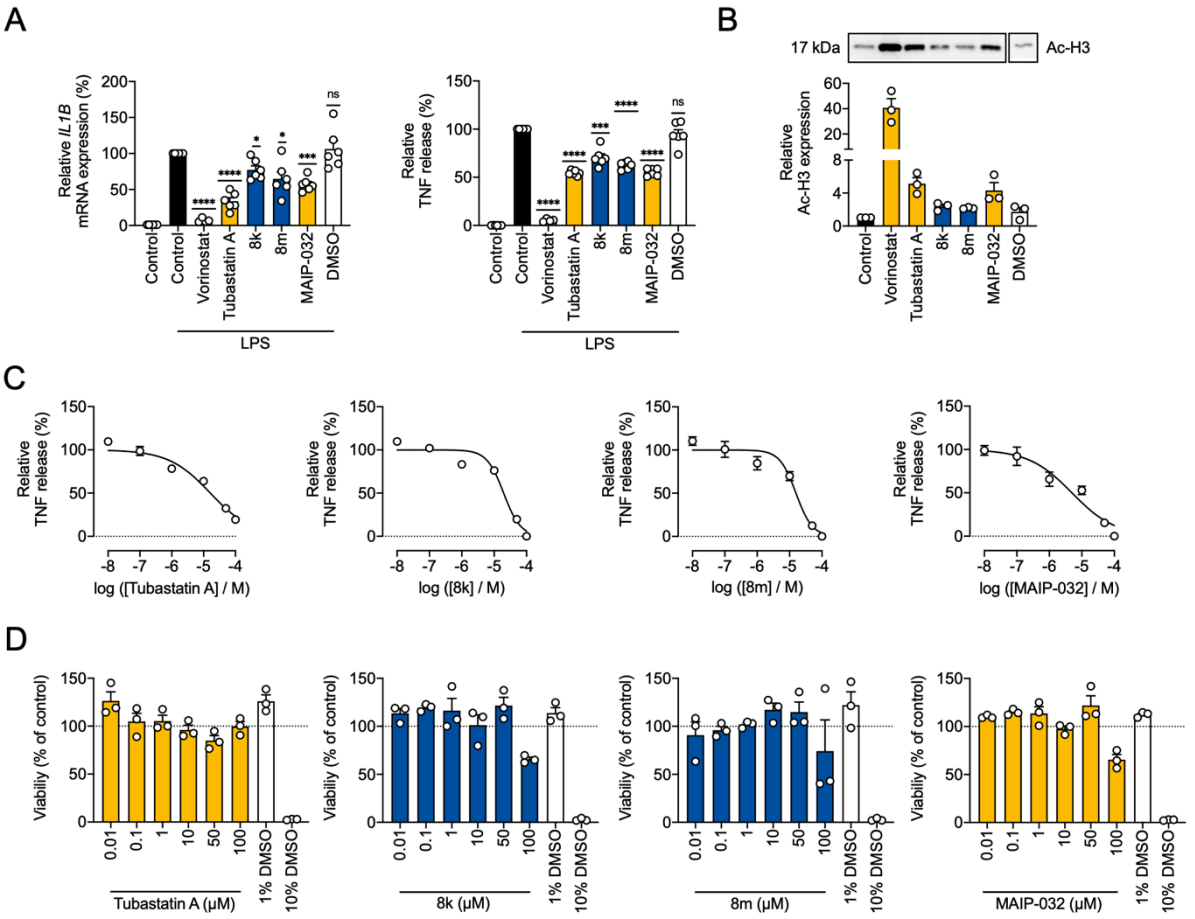

Figure 6. (**A**) Human THP-1 macrophages were incubated with indicated HDAC inhibitors (10 µM) or vehicle (0.1%, v/v, DMSO) for 24 h. Subsequently, cells were incubated with LPS (100 ng/ml) for 3h. Supernatants were assayed for TNF release by ELISA. *IL1B* gene expression was normalized to the housekeeping gene *GAPDH*. LPS induced TNF release and *IL1B* gene expression was set to 100%. Other values were calculated accordingly. Mean + SEM, n=4-6. One sample t test against 100 %. ns = not significant, *P ≤ 0.05, ***P ≤ 0.001, ****P ≤ 0.0001. (**B**) Human THP-1 macrophages were incubated with indicated HDAC inhibitors (10 µM) or vehicle (0.1%, v/v, DMSO) for 24 h. Cell lysates were analyzed for acetyl-histone-H3 expression by western blot. Acetyl-histone-H3 protein levels were normalized to the respective total protein amount and values were referenced to the control (control set to a value of 1). Mean + SEM, n=3. (**C**) Human THP-1 macrophages were incubated with increasing concentrations of indicated HDAC inhibitors for 24 h. Subsequently, cells were incubated with LPS (100 ng/ml) for 3 h. Supernatants were assayed for TNF release by ELISA. LPS induced TNF release was set to 100%. Other values were calculated accordingly. Mean ± SEM, n=3-4. Curves were fitted to a monophasic model with variable slope. (**D**) Human THP-1 macrophages were incubated with increasing concentrations of indicated HDAC inhibitors for 24 h. DMSO (1% and 10%, v/v) served as controls. Cytotoxicity was determined by MTT assay. Mean + SEM, n=3.

Next, we analyzed the inhibitory potency of the HDAC6 inhibitors on LPS-induced TNF release (Figure 6C). To determine whether the data for the tested inhibitors, tubastatin A, **MAIP-032**, **8k**, and **8m**, were better represented by a monophasic or biphasic inhibitory concentration-response curve, we conducted a comparative analysis of both models. Tubastatin A, **MAIP-032** and **8m** were best fitted by a monophasic model, while a biphasic model was preferred for **8k**. However, for better comparison all inhibitors were fitted to monophasic inhibitory concentration-response curves with IC_{50} values ranging from 4.96 to 19.6 µM (Table 4).

Table 4. Inhibitory activities of **8k**, **8m**, **MAIP-032**, and tubastatin A against LPS-induced TNF release by THP-1 macrophages. [a]

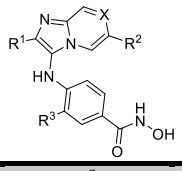

entry	R^1	R^2	R^3	IC_{50} [µM] (95% CI)
8k (X = CH)	Propyl	H	F	19.6 (15.4-25.2)
8m (X = CH)	Methyl	H	F	15.8 (11.0-22.3)
MAIP-032 (X = CH)	Propyl	H	H	4.96 (2.34-9.97)
Tubastatin A	/	/	/	16.3 (10.6-24.2)

[a]Stated IC_{50} values were determined from the mean of at least three independent experiments.

IC_{50} values of **8k** (19.6 µM) and **8m** (15.8 µM) were similar to tubastatin A (16.3 µM), but all three compounds appear to be less potent than **MAIP-032** (4.96 µM). Cell viability in the presence of the HDAC6 inhibitors remained unchanged up to 50 µM and was reduced to 60% at 100 µM for **MAIP-032**, **8k**, and **8m** (Figure 6D). The possibility of a biphasic fit indicates that at least two HDAC6-mediated mechanisms contribute to the inhibition of LPS-induced TNF release. HDAC6 inhibitors affect TLR signaling by modulating acetylation of several proteins involved in this pathway, among other mechanisms.[43] However, the specific mechanistic details remain poorly understood. Further studies are warranted to clarify the underlying mechanisms behind the inhibitory role of HDAC6 in TLR-mediated priming.

3 Conclusions

In this study, starting from a co-crystal structure of the preferential HDAC6 inhibitor **MAIP-032**, we performed a structure-based optimization campaign to yield a series of inhibitors with improved potency and selectivity. The synthesis of 13 novel inhibitors was achieved using a highly efficient *Groebke Blackburn Bienaymé* three component reaction as the key step. While the variation of the propyl group of **MAIP-032** showed only a slight improvement in HDAC6 selectivity (e.g. compound **8a**), the fluorination of the benzyl linker in *meta*-position to

the hydroxamic acid significantly enhanced potency and selectivity (compounds **8k** and **8m**). Compound **8k** outperformed the gold standard selective HDAC6 inhibitor, tubastatin A, in terms of selectivity. Importantly, **8k** and **8m** exhibit notable selectivity over HDAC10, the closest paralog of HDAC6. This finding is crucial as inhibiting HDAC10 can potentially counteract the anti-inflammatory processes mediated by the inhibition of HDAC6.[31,32] While neither **8k** and **8m** nor tubastatin A demonstrated pronounced antiproliferative effects in the U-87 MG glioblastoma cell line, compound **8m** effectively attenuated cell migration in wound healing assays. Additionally, tubastatin A, **MAIP-032**, **8k**, and **8m** showed significant inhibition of LPS-induced *IL1B* mRNA expression and TNF release in macrophages, thereby indicating that our imidazo[1,2-a]pyridine-capped HDAC6 inhibitors could be a suitable starting to develop drugs to treat NLRP3 inflammasome driven inflammatory diseases.

4 Experimental section

4.1 General Information & Chemistry

Chemicals were obtained from abcr GmbH, Acros Organics, Carbolution Chemicals, Fluorochem, Sigma-Aldrich, TCI Chemicals or VWR and used without further purification. Technical grade solvents were distilled prior to use. For all HPLC purposes, acetonitrile in HPLC-grade quality (HiPerSolv CHROMANORM, *VWR*) was used. Water was purified with a PURELAB flex® (*ELGA VEOLIA*). Air-sensitive reactions were carried out under argon atmosphere utilizing standard *Schlenk* techniques. If no solvent is stated an aqueous solution was prepared with demineralized water. Mixtures of two or more solvents are specified as "solvent A"/"solvent B", 3/1, *v*/*v*; meaning that 100 mL of the respective mixture consists of 75 mL of "solvent A" and 25 mL of "solvent B". **Thin-layer chromatography (TLC)** was carried out on prefabricated plates (silica gel 60, F_{254}, *Merck*). Components were visualized either by irradiation with ultraviolet light (254 nm or 366 nm) or by staining appropriately. **Column Chromatography:** If not stated otherwise, column chromatography was carried out on silica gel (60 Å, 40-60 µm, *Acros Organics*). **Melting Point (mp.):** The uncorrected melting points were determined using a *Büchi* Melting Point M-560 apparatus. **Nuclear Magnetic Resonance Spectroscopy (NMR):** Proton (^{1}H), carbon (^{13}C), and fluorine (^{19}F) NMR spectra were recorded either on Bruker Avance III HD 400 MHz at a frequency of 400 MHz (^{1}H), 100 MHz (^{13}C) and 377 MHz (^{19}F), a *Varian/Agilent* Mecury-plus-400 at a frequency of 400 MHz (^{1}H) and 100 MHz (^{13}C), a *Varian/Agilent* Mecury-plus-300 at a frequency of 300 MHz (^{1}H), 75 MHz (^{13}C) and 282 MHz (^{19}F) , a *Bruker* AVANCE 500 MHz at a frequency of 500 MHz (^{1}H) and 126 MHz (^{13}C) or on a *Bruker* AVANCE III HD 600 MHz at a frequency of 600 MHz (^{1}H), 151 MHz (^{13}C) and 565 MHz (^{19}F). The chemical shifts are given in parts per million (ppm). As solvents deuterated chloroform ($CDCl_3$), deuterated methanol (MeOH-d_4) and

deuterated dimethyl sulfoxide (DMSO-d_6) were used. The residual solvent signal ($CDCl_3$: ^{1}H NMR: 7.26 ppm, ^{13}C NMR: 77.1 ppm; DMSO-d_6: ^{1}H NMR: 2.50 ppm, ^{13}C NMR: 39.52 ppm; MeOH-d_4: ^{1}H NMR: 3.31 ppm, 4.87 ppm, ^{13}C NMR: 49.00 ppm) was used for calibration. The multiplicity of each signal is reported as singulet (s), doublet (d), triplet (t), quartet (q), pentet (p), sextet (sext), multiplet (m) or combinations thereof. Multiplicities and coupling constants are reported as measured and might disagree with the expected values. **Mass Spectrometry:** High resolution electrospray ionization mass spectra (HRMS-ESI) were acquired with *Bruker Daltonik GmbH* micrOTOF coupled to a an *LC Packings* Ultimate HPLC system and controlled by micrOTOFControl3.4 and HyStar 3.2-LC/MS, with a *BrukerDaltonik GmbH* ESI-qTOF Impact II coupled to a *Dionex* UltiMateTM 3000 UHPLC system and controlled by micrOTOFControl 4.0 and HyStar 3.2-LC/MS or with a micrOTOF-Q mass spectrometer (*Bruker*) with ESI-source coupled with an HPLC Dionex UltiMate 3000 (*Thermo Scientific*). Low resolution electrospray ionisation mass spectra (LRMS-ESI) were acquired with an *Advion* expression® compact mass spectrometer (CMS) coupled with an automated TLC plate reader Plate Express® (*Advion*). **High Performance Liquid Chromatography (HPLC)**: A *Thermo Fisher Scientific* UltiMate^{TM} 3000 UHPLC system with a Nucleodur 100-5 C18 (250 x 4.6 mm, *Macherey Nagel*) with a flow rate of 1 mL/min and a temperature of 25 °C or a 100-5 C18 (100 x 3 mm, *Macherey Nagel*) with a flow rate of 0.5 mL/min and a temperature of 25 °C with an appropriate gradient were used. For preparative purposes a AZURA Prep. 500/1000 gradient system (*Knauer*) with a Nucleodur 110-5 C18 HTec (150 x 32 mm, *Macherey Nagel*) column with 20 mL/min was used. Detection was implemented by UV absorption measurement at a wavelength of λ = 220 nm and λ = 250 nm. Bidest. H_2O (A) and MeCN (B) were used as eluents with an addition of 0.1% TFA for eluent A. **Purity:** The purity of all final compounds was 95% or higher. Purity was determined via HPLC with the Nucleodur 100-5 C18 (250 x 4.6 mm, *Macherey Nagel*) at 250 nm. After column equilibration for 5 min a linear gradient from 5% A to 95% B in 7 min followed by an isocratic regime of 95% B for 10 min was used.

4.2 Experimental procedures (chemistry)

4.2.1 General procedures

General procedure I (GP I): The respective amine (1.00 eq) was dissolved in formic acid (20.0 eq.) and ethyl acetate (1.5 mL). The solution was stirred for three days at room temperature before the solvent was removed under reduced pressure. The residue was dissolved in ethyl acetate (50 mL) and washed with H_2O (50 mL). The inorganic layer was extracted with ethyl acetate (3 x 20 mL). The combined organic layers were washed with sat.

$NaHCO_3$-solution (20 mL) and sat. NaCl-solution (20 mL) and dried over Na_2SO_4. After evaporation of the solvent under reduced pressure the respective formamide was isolated and used without further purification.

General procedure II (GP II): The respective formamide (1.00 eq.) was dissolved in CH_2Cl_2 (0.25 M) and NEt_3 (3.00 eq.) was added. The solution was cooled to 0 °C and phenyl phosphordichloridate (1.20 eq) was added dropwise over 5 min. The ice bath was removed and the solution stirred for 90 min at rt. The solvent was removed under reduced pressure and the residue purified by column chromatography (Al_2O_3 neutral BROCKMANN Grade I, CyH/CH_2Cl_2 1:4, *v*/*v*).

General procedure III (GP III): The respective amidine (1.00 eq.) and aldehyde (1.10 eq.) were dissolved in MeOH (0.3 M). Acetic acid (2.00 eq.) was added, and the solution stirred for 30 min at rt. Next, the respective isocyanate (1.00 eq.) was added, and the suspension submitted to microwave irritation (110 W) for 3 h at 85 °C. Afterwards, the solvent was removed under reduced pressure and the residue was purified by column chromatography.

General procedure IV (GP IV): The respective ester (1.00 eq.) was dissolved in CH_2Cl_2/MeOH (0.25 M, 1:2, *v*/*v*) and cooled to 0 °C. Hydroxyl amine (50% in H_2O, 30.0 eq.,) and NaOH (10.0 eq.) were added and the reaction mixture was stirred for 30 min at 0 °C followed by 60 min at rt. Subsequently, the solvent was removed under reduced pressure and the residue was taken up in a small amount of water. The pH value of the aqueous solution adjusted to 7–8 using 1 M HCl, the precipitated solid filtrated, washed with Et_2O (3 x 5 mL) and dried *in vacuo*.

4.2.2 Compound characterization

Methyl-4-formamidobenzoate (**1**)

Prepared according to **GP I**. Starting from methyl-4-aminobenzoate (3.12 g, 20.6 mmol, 1.00 eq.). Compound **1** (3.69 g, 20.6 mmol, quant.) was isolated as a beige solid. **R_f** (CyH/EE 2:1, *v*/*v*) = 0.12; **^{1}H NMR** (300 MHz, $CDCl_3$) δ = 8.84 (d, *J* = 11.2 Hz, 1H), 8.44 (d, *J* = 1.6 Hz, 1H), 8.14 (s, 1H), 8.09 – 7.97 (m, 3H), 7.74 – 7.57 (m, 2H), 7.47 (s, 1H), 7.20 – 7.07 (m, 1H), 3.91 (s, 2H), 3.90 (s, 3H); **LRMS-ESI (*m/z*):** $[M+H]^+$ calcd for $C_9H_9NO_3$: 180.1, found: 180.1. Analytical data match with literature.[37]

Methyl-3-fluoro-4-formamidobenzoate (**2**)

Prepared according to **GP I**. Starting from methyl-3-fluoro-4-aminobenzoate (1.69 g, 10.0 mmol, 1.00 eq.). Compound **2** (1.86 g, 9.43 mmol, 94%) was isolated as a beige solid. **R_f** (CyH/EE 2:1, *v*/*v*) = 0.3; **mp.** 154-156 °C; **^{1}H NMR** (300 MHz, $CDCl_3$) δ = 8.90 – 8.80 (m, 1H), 8.58 – 8.40 (m, 1H), 7.89 – 7.66 (m, 3H), 7.36 – 7.28 (m,

1H), 3.91 (s, 3H); **^{13}C NMR** (101 MHz, $CDCl_3$) δ = 165.7, 161.0, 158.9, 151.4 (d, *J* = 244.3 Hz), 129.8 (d, *J* = 10.3 Hz), 126.9 – 126.5 (m), 121.2, 118.1 – 117.6 (m), 117.3, 116.5 – 115.9 (m), 52.8 – 52.2 (m); **^{19}F NMR** (282 MHz $CDCl_3$) δ = -128.8 – -128.9 (m), -130.8 – -131.2 (m); **LRMS-ESI (*m/z*):** $[M+Na]^+$ calcd for $C_9H_8FNO_3$: 220.0, found: 220.0.

Methyl-4-formamido-3-methylbenzoate (**3**)

Prepared according to **GP I**. Starting from methyl-4-amino-3-methylbenzoate (0.825 g, 5.00 mmol, 1.00 eq.). Compound **3** (0.935 g, 4.83 mmol, 97%) was isolated as a white solid. **R_f** (CyH/EE 1:1, *v*/*v*) = 0.44; **mp.** 120 – 122 °C; **^{1}H NMR** (600 MHz, $CDCl_3$) δ = 8.72 (d, *J* = 11.1 Hz, 1H), 8.50 (d, *J* = 1.7 Hz, 0H), 8.20 (d, *J* = 8.3 Hz, 0H), 7.98 – 7.84 (m, 3H), 7.30 (s, 1H), 7.21 (d, *J* = 8.3 Hz, 1H), 3.90 (d, *J* = 7.1 Hz, 3H), 2.33 (d, *J* = 6.4 Hz, 3H); **^{13}C NMR** (151 MHz, $CDCl_3$) δ = 166.8, 166.6, 162.5, 159.1, 139.3, 139.2, 132.9, 132.0, 129.0, 128.8, 128.0, 127.1, 126.7, 126.3, 121.3, 118.1, 53.1, 52.1,17.7; **LRMS-ESI (*m/z*):** $[M+H]^+$ calcd for $C_{10}H_{12}NO_3$: 194.1 found: 194.1.

Methyl-4-isocyanobenzoate (**4**)

Prepared according to **GP II**. Starting from formamide **1** (1.06 g, 5.92 mmol, 1.00 eq.). Compound **4** (0.899 g, 5.59 mmol, 94%) was isolated as a dark green solid. **R_f** (CyH/CH_2Cl_2 1:4, *v*/*v*) = 0.68; **mp.** ~30 °C; **^{1}H NMR** (300 MHz, $CDCl_3$) δ = 8.14 – 8.02 (m, 2H), 7.50 – 7.38 (m, 2H), 3.94 (s, 3H); **LRMS-ESI (*m/z*):** $[M+H]^+$ calcd for $C_9H_8NO_2$: 162.1, found: 162.0. Analytical data match with literature.[37]

Methyl-3-fluoro-4-isocyanobenzoate (**5**)

Prepared according to **GP II**. Starting from formamide **2** (0.986 g, 4.99 mmol, 1.00 eq.). Compound **5** (0.548 g, 3.06 mmol, 61%) was isolated as a brown solid. **R_f** (CyH/CH_2Cl_2 1:4, *v*/*v*) = 0.68, **mp.** ~30 °C; **^{1}H NMR** (300 MHz, $CDCl_3$) δ = 7.89 – 7.87 (m, 1H), 7.86 – 7.83 (m, 1H), 7.53 – 7.44 (m, 1H), 3.95 (s, 3H); **^{13}C NMR** (101 MHz, $CDCl_3$) δ = 173.3, 164.7, 157.2 (d, *J* = 258.4 Hz), 132.9 (d, *J* = 6.5 Hz), 128.1, 126.0 (d, *J* = 4.0 Hz), 118.0 (d, *J* = 20.3 Hz), 53.0; **^{19}F NMR** (377 MHz, $CDCl_3$) δ -116.6 (d, *J* = 5.2 Hz); **LRMS-ESI (*m/z*):** $[M+K]^+$ calcd for $C_9H_6FNO_2$: 218.0, found: 218.0.

Methyl-4-isocyano-3-methylbenzoate (**6**)

Prepared according to **GP II**. Starting from formamide **3** (0.560 g, 3.00 mmol, 1.00 eq.). Compound **6** (0.431 g, 2.46 mmol, 82%) was isolated as a white solid. **R_f** (CyH/CH_2Cl_2 1:4, *v*/*v*) = 0.70; **mp.** ~30 °C; **^{1}H NMR** (600 MHz, $CDCl_3$) δ = 7.97 (s, 1H), 7.88 (dd, *J* = 8.2, 1.9 Hz, 1H), 7.40 (d, *J* = 8.3 Hz, 1H), 3.92 (s, 3H), 2.48 (s, 3H);

^{13}C NMR (151 MHz, $CDCl_3$) δ = 168.7, 165.9, 135.4, 131.9, 130.8, 130.4 – 129.7 (m), 128.1, 126.7, 52.6, 18.7; **LRMS-ESI (*m/z*):** $[M+H]^+$ calcd for $C_{10}H_9NO_2$: 176.1, found: 176.1.

Methyl-4-[(2-methylimidazo[1,2-a]pyridin-3-yl)amino]benzoate (**7a**)

Prepared according to **GP III**. Starting from 2-aminopyridine (0.103 g, 1.10 mmol, 1.00 eq.), acetaldehyde (5 M in THF, 0.240 mL, 52.8 mg, 1.20 mmol, 1.10 eq.), isonitrile **4** (0.181 g, 1.10 mmol, 1.00 eq.), and acetic acid (0.125 mL, 0.132 g, 2.20 mmol, 2.00 eq.). The crude mixture was purified by column chromatography (CyH/EE 2:1 to 0:1 *v*/*v*). Compound **7a** (0.164 g, 0.583 mmol, 53%) was isolated as a brown solid. **R_f** (CyH/EE 1:4, *v*/*v*) = 0.10; **mp.** 187 – 189 °C; **^{1}H NMR** (500 MHz, DMSO-d_6) δ = 8.49 (s, 1H), 7.88 (dt, *J* = 6.8, 1.2 Hz, 1H), 7.79 – 7.74 (m, 2H), 7.49 (dt, *J* = 9.0, 1.1 Hz, 1H), 7.22 (ddd, *J* = 9.0, 6.7, 1.3 Hz, 1H), 6.86 (td, *J* = 6.7, 1.1 Hz, 1H), 6.52 (d, *J* = 8.4 Hz, 2H), 3.76 (s, 3H), 2.22 (s, 3H); **^{13}C NMR** (126 MHz, DMSO-d_6) δ = 166.0, 150.7, 141.5, 137.1, 131.3, 124.0, 122.6, 119.0, 118.0, 116.5, 112.3, 111.7, 51.4, 12.7; **LRMS-ESI (*m/z*)**: $[M+H]^+$ calcd for $C_{16}H_{15}N_3O_2$: *282.1*, found: 282.2.

Methyl 4-[(2-ethylimidazo[1,2-a]pyridin-3-yl)amino]benzoate (**7b**)

Prepared according to **GP III**. Starting from 2-aminopyridine (0.103 g, 1.10 mmol, 1.00 eq.), propionaldehyde (0.128 mL, 0.104 g, 1.20 mmol, 1.09 eq.), isonitrile **4** (0.181 g, 1.10 mmol, 1.00 eq.), and acetic acid (0.125 mL, 0.132 g, 2.20 mmol, 2.00 eq.). The crude mixture was purified by column chromatography (CyH/EE 2:1 to 1:4 *v*/*v*). Compound **7b** (0.166 g, 0.562 mmol, 51%) was isolated as a green solid. **R_f** (CyH/EE 1:1, *v*/*v*) = 0.10; **mp.** 160 – 162 °C; **^{1}H NMR** (400 MHz, DMSO-d_6) δ = 8.01 – 7.88 (m, 2H), 7.58 (d, *J* = 8.1 Hz, 2H), 7.15 (d, *J* = 8.1 Hz, 2H), 7.13 – 7.08 (m, 1H), 6.71 – 6.59 (m, 1H), 4.32 (s, 2H), 3.89 (s, 3H), 2.80 (t, *J* = 7.6 Hz, 2H), 1.82 (q, *J* = 7.5 Hz, 2H), 0.99 (t, *J* = 7.3 Hz, 3H); **^{13}C NMR** (101 MHz, DMSO-d_6) δ = 166.1, 150.9, 142.5, 141.6, 131.3, 124.0, 122.7, 119.0, 117.2, 116.7, 112.3, 111.8, 51.5, 20.1, 13.5; **HRMS-ESI (m/z)**: $[M+H]^+$ calcd for $C_{17}H_{17}N_3O_2$: 296,1404, found: 296,1399.

Methyl 4-[(2-*iso*-butylimidazo[1,2-a]pyridin-3-yl)amino]benzoate (**7c**)

Prepared according to **GP III**. Starting from 2-aminopyridine (0.103 g, 1.10 mmol, 1.00 eq.), isovaleraldehyde, isonitrile **4** (0.181 g, 1.10 mmol, 1.00 eq.), and acetic acid (0.125 mL, 0.132 g, 2.20 mmol, 2.00 eq.). The crude mixture was purified by column chromatography (CyH/EE 2:1 to 1:2 *v*/*v*). Compound **7c** (0.234 g, 0.723 mmol, 66%) was isolated as a brown solid. **R_f** (CyH/EE 1:1, *v*/*v*) = 0.14; **mp.** 72 – 74 °C; **^{1}H NMR** (400 MHz, DMSO-d_6) δ = 8.51 (s, 1H), 7.83 (d, *J* = 6.7 Hz, 1H), 7.75 (d, *J* = 8.5 Hz, 2H), 7.52 (d, *J* = 9.0 Hz, 1H), 7.31 – 7.16 (m, 1H), 6.91 – 6.80 (m, 1H), 6.49 (d, *J* = 8.4 Hz, 2H), 3.75 (s, 3H), 2.45 (d, *J* = 7.1 Hz, 2H), 2.06 (hept, *J* = 6.7 Hz,

1H), 0.85 (d, J = 6.6 Hz, 6H); **^{13}C NMR** (75 MHz, DMSO-d_6) δ = 166.5, 151.2, 142.1, 141.1, 131.7, 124.5, 123.1, 119.4, 118.7, 117.2, 112.8, 112.2, 51.9, 36.3, 28.2, 23.0; **HRMS-ESI (m/z)**: $[M+H]^+$ calcd for $C_{19}H_{21}N_3O_2$: 324.1712, found: 324.1709.

Methyl 4-[(2-cyclopropylimidazo[1,2-a]pyridin-3-yl)amino]benzoate (**7d**)

Prepared according to **GP III**. Starting from 2-aminopyridine (0.103 g, 1.10 mmol, 1.00 eq.), (89.0 µL, 83.4 mg, 1.17 mmol, 1.06 eq.) cyclopropanal, isonitrile **4** (0.181 g, 1.10 mmol, 1.00 eq.), and acetic acid (0.125 mL, 0.132 g, 2.20 mmol, 2.00 eq.). The crude mixture was purified by column chromatography (CyH/EE 2:1 to 1:3 *v*/*v*). Compound **7d** (0.282 g, 0.917 mmol, 84%) was isolated as a brown solid. **R_f** (CyH/EE 1:2, *v*/*v*) = 0.18; **mp.** 194 – 196 °C; **^{1}H NMR** (400 MHz, DMSO-d_6) δ = 8.58 (s, 1H), 7.85 (dt, *J* = 6.8, 1.2 Hz, 1H), 7.77 (d, 2H), 7.51 – 7.41 (m, 1H), 7.25 – 7.15 (m, 1H), 6.87 – 6.80 (m, 1H), 6.55 (d, *J* = 8.3 Hz, 2H), 3.76 (s, 3H), 1.87 (ddt, *J* = 9.8, 8.1, 4.3 Hz, 1H), 0.89 (dtd, *J* = 17.6, 5.9, 3.4 Hz, 4H); **^{13}C NMR** (101 MHz, DMSO-d_6) δ = 166.1, 150.9, 142.3, 141.6, 131.3, 124.0, 122.4, 119.0, 117.5, 116.4, 112.4, 111.7, 51.5, 8.0, 7.9; **HRMS-ESI (*m*/*z*)**: $[M+H]^+$ calcd for $C_{18}H_{17}N_3O_2$: 308.1399, found: 308.1399.

Methyl 4-[(2-butylimidazo[1,2-a]pyridin-3-yl)amino]benzoate (**7e**)

Prepared according to **GP III**. Starting from 2-aminopyridine (0.103 g, 1.10 mmol, 1.00 eq.), valeraldehyde (0.161 mL, 0.129 g, 1.20 mmol, 1.09 eq.), isonitrile **4** (0.181 g, 1.10 mmol, 1.00 eq.), and acetic acid (0.125 mL, 0.132 g, 2.20 mmol, 2.00 eq.). The crude mixture was purified by column chromatography (CyH/EE 2:1 to 1:2 *v*/*v*). Compound **7e** (0.142 g, 0.439 mmol, 40%) was isolated as a brown solid. **R_f** (CyH/EE 1:1, *v*/*v*) = 0.20; **mp.** 98 – 100 °C; **^{1}H NMR** (400 MHz, DMSO-d_6) δ = 8.50 (s, 1H), 7.87 (d, *J* = 6.7 Hz, 1H), 7.76 (d, *J* = 8.5 Hz, 2H), 7.51 (d, *J* = 9.0 Hz, 1H), 7.28 – 7.18 (m, 1H), 6.91 – 6.82 (m, 1H), 6.50 (d, *J* = 8.3 Hz, 2H), 3.75 (s, 3H), 2.58 (q, *J* = 7.6 Hz, 2H), 1.19 (t, *J* = 7.5 Hz, 3H); **^{13}C NMR** (101 MHz, DMSO-d_6) δ = 166.1, 150.9, 142.5, 141.6, 131.3, 124.0, 122.7, 119.0, 117.2, 116.7, 112.3, 111.8, 51.5, 20.1, 13.5; **HRMS-ESI (m/z)**: $[M+H]^+$ calcd for $C_{19}H_{21}N_3O_2$: 324.1712, found: 324.1714.

Methyl 4-[(2-pentylimidazo[1,2-a]pyridin-3-yl)amino]benzoate (**7f**)

Prepared according to **GP III**. Starting from 2-aminopyridine (0.103 g, 1.10 mmol, 1.00 eq.), hexanal (0.142 mL, 0.129 g, 1.20 mmol, 1.09 eq.), isonitrile **4** (0.181 g, 1.10 mmol, 1.00 eq.), and acetic acid (0.125 mL, 0.132 g, 2.20 mmol, 2.00 eq.). The crude mixture was purified by column chromatography (CyH/EE 2:1 to 1:2 *v*/*v*). Compound **7f** (0.159 g, 0.471 mmol, 43%) was isolated as a brown solid. **R_f** (CyH/EE 1:1, *v*/*v*) = 0.28; **mp.** 55 – 57 °C; **^{1}H NMR** (300 MHz, DMSO-d_6) δ = 8.50 (s, 1H), 7.88 – 7.82 (m, 1H), 7.75 (d, *J* = 8.9 Hz, 2H), 7.54 – 7.47

(m, 1H), 7.26 – 7.17 (m, 1H), 6.89 – 6.81 (m, 1H), 6.49 (d, *J* = 8.4 Hz, 2H), 3.75 (s, 3H), 2.56 (t, *J* = 7.5 Hz, 2H), 1.70 – 1.57 (m, 2H), 1.26 – 1.18 (m, 4H), 0.81 – 0.74 (m, 3H); **^{13}C NMR** (75 MHz, DMSO-d_6) δ = 166.1, 150.9, 141.6, 141.4, 131.2, 124.0, 122.6, 119.0, 117.7, 116.7, 112.3, 111.8, 51.4, 31.0, 28.1, 26.5, 21.8, 13.8; **HRMS-ESI (m/z)**: $[M+H]^+$ calcd for $C_{20}H_{23}N_3O_2$: 338.1869, found: 338.1870.

Methyl 4-{[2-(3,3,3-trifluoropropyl)imidazo[1,2-a]pyridin-3-yl]amino}benzoate (**7g**)

Prepared according to **GP III**. Starting from 2-aminopyridine (0.103 g, 1.10 mmol, 1.00 eq.), 4,4,4-trifluorbutanal (0.116 mL, 0.139 g, 1.20 mmol, 1.09 eq.), isonitrile **4** (0.181 g, 1.10 mmol, 1.00 eq.), and acetic acid (0.125 mL, 0.132 g, 2.20 mmol, 2.00 eq.). The crude mixture was purified by column chromatography (CyH/EE 2:1 to 0:1 *v*/*v*). Compound **7g** (0.185 g, 0.509 mmol, 47%) was isolated as an orange solid. **R_f** (CyH/EE 1:1, *v*/*v*) = 0.11; **mp.** 183 – 185 °C; **^{1}H NMR** (400 MHz, DMSO-d_6) δ = 8.55 (s, 1H), 7.90 (dt, *J* = 6.8, 1.2 Hz, 1H), 7.83 – 7.72 (m, 2H), 7.55 (dt, *J* = 9.0, 1.1 Hz, 1H), 7.27 (ddd, *J* = 9.0, 6.7, 1.3 Hz, 1H), 6.90 (td, *J* = 6.8, 1.2 Hz, 1H), 6.53 (d, *J* = 8.3 Hz, 2H), 3.76 (s, 3H), 2.82 (dd, *J* = 9.9, 6.0 Hz, 2H), 2.74 – 2.59 (m, 2H); **^{13}C NMR** (101 MHz, DMSO-d_6) δ = 166.0, 150.5, 141.7, 137.9, 131.3, 127.3 (q, *J* = 276.8 Hz), 124.5, 122.9, 119.3, 118.0, 116.8, 112.4, 112.2, 51.5, 31.7 (q, *J* = 27.7 Hz), 19.5; **^{19}F {^{1}H} NMR** (377 MHz, DMSO-d_6) δ = -65.2 (s); **HRMS-ESI (*m*/*z*)**: $[M+H]^+$ calcd for $C_{18}H_{16}F_3N_3O_2$: 364.1273, found: 364.1273.

Methyl 4-[(6-methyl-2-propylimidazo[1,2-a]pyridin-3-yl)amino]benzoate (**7h**)

Prepared according to **GP III**. Starting from 5-methyl-2-aminopyridine (0.119 g 1.10 mmol, 1.00 eq.), butanal (0.108 mL, 86.5 mg, 1.20 mmol, 1.10 eq.), isonitrile **4** (0.181 g, 1.10 mmol, 1.00 eq.), and acetic acid (0.125 mL, 0.132 g, 2.20 mmol, 2.00 eq.). The crude mixture was purified by column chromatography (CyH/EE 1:2 to 1:9 *v*/*v*). Compound **7h** (0.150 g, 0.464 mmol, 42%) was isolated as a brown solid. **R_f** (CyH/EE 1:2, *v*/*v*) = 0.18; **mp.** 175 – 176 °C; **^{1}H NMR** (400 MHz, DMSO-d_6) δ = 8.45 (s, 1H), 7.79 – 7.68 (m, 3H), 7.28 (s, 1H), 6.70 (dd, *J* = 6.9, 1.6 Hz, 1H), 6.49 (d, *J* = 8.3 Hz, 2H), 3.75 (s, 3H), 2.54 – 2.51 (m, 1H), 2.34 (s, 3H), 1.64 (sext, *J* = 7.4 Hz, 2H), 0.85 (t, *J* = 7.4 Hz, 3H); **^{13}C NMR** (101 MHz, DMSO-d_6) δ = 166.1, 151.0, 142.0, 140.8, 134.5, 131.2, 122.0, 118.9, 117.2, 115.1, 114.2, 112.2, 51.4, 28.7, 21.8, 20.7, 13.9; **HRMS-ESI (*m*/*z*)**: $[M+H]^+$ calcd for $C_{19}H_{21}N_3O_2$: 324.1714, found: 324.1750.

Methyl 4-[(6-ethyl-2-propylimidazo[1,2-a]pyridin-3-yl)amino]benzoate (**7i**)

Prepared according to **GP III**. Starting from 5-ethyl-2-aminopyridine (0.134 g, 1.10 mmol, 1.00 eq.), butanal (0.108 mL, 86,5 mg, 1.20 mmol, 1.10 eq.), isonitrile **4** (0.181 g, 1.10 mmol, 1.00 eq.), and acetic acid (0.125 mL, 0.132 g, 2.20 mmol, 2.00 eq.). The crude mixture was purified by column chromatography (CyH/EE 1:2 to 1:9

v/*v*). Compound **7i** (0.157 g, 0.465 mmol, 42%) was isolated as a brown solid. **R_f** (CyH/EE 1:2, *v*/*v*) = 0.18; **mp.** 161 – 163 °C; **^{1}H NMR** (400 MHz, DMSO-d_6) δ = 8.46 (s, 1H), 7.80 – 7.70 (m, 3H), 7.29 (s, 1H), 6.75 (dd, *J* = 7.0, 1.7 Hz, 1H), 6.49 (d, *J* = 8.3 Hz, 2H), 3.75 (s, 3H), 2.68 – 2.61 (m, 2H), 2.53 (d, *J* = 7.3 Hz, 2H), 1.64 (h, *J* = 7.4 Hz, 2H), 1.21 (t, *J* = 7.5 Hz, 3H), 0.85 (t, *J* = 7.4 Hz, 3H); **^{13}C NMR** (75 MHz, DMSO-d_6) δ = 166.1, 151.0, 142.0, 140.9, 140.6, 131.2, 122.2, 118.9, 117.2, 113.7, 113.2, 112.3, 51.4, 28.7, 27.6, 21.8, 14.6, 13.9; **HRMS-ESI** (*m*/*z*): $[M+H]^+$ calcd for $C_{20}H_{23}N_3O_2$: 338.1869, found: 338.1906.

Methyl 4-[(2-propylimidazo[1,2-a]pyrazin-3-yl)amino]benzoate (**7j**)

Prepared according to **GP III**. Starting from 2-aminopyrazine (0.143 g, 1.50 mmol, 1.00 eq.), (0.149 mL, 0.119 g, 1.65 mmol, 1.10 eq.) butanal, isonitrile **4** (0.241 g, 1.50 mmol, 1.00 eq.), and acetic acid (0.171 mL, 0.180 g, 3.00 mmol, 2.00 eq.). The crude mixture was purified by column chromatography (CH_2Cl_2/MeOH 1:0 to 95:5 *v*/*v*). Compound **7j** (0.185 g, 0.596 mmol, 40%) was isolated as a yellow solid. **R_f** (CH_2Cl_2/MeOH 99:1, *v*/*v*) = 0.20; **mp.** 161 – 163 °C; **^{1}H NMR** (300 MHz, DMSO-d_6) δ = 8.98 (d, *J* = 1.5 Hz, 1H), 8.69 (s, 1H), 7.95 (dd, *J* = 4.5, 1.5 Hz, 1H), 7.84 (d, *J* = 4.5 Hz, 1H), 7.80 – 7.74 (m, 2H), 6.57 – 6.49 (m, 2H), 3.76 (s, 3H), 2.61 (t, *J* = 7.9 Hz, 2H), 1.68 (sext, *J* = 7.4 Hz, 2H), 0.85 (t, *J* = 7.3 Hz, 3H); **^{13}C NMR** (101 MHz, DMSO-d_6) δ = 166.0, 150.0, 143.8, 142.2, 137.1, 131.3, 129.0, 119.7, 119.5, 116.2, 112.6, 51.5, 28.7, 21.5, 13.8; **HRMS-ESI (*m*/*z*)**: $[M+H]^+$ calcd for $C_{17}H_{18}N_4O_2$: 311.1508, found: 311.1505.

Methyl-3-fluoro-4-[(2-propylimidazo[1,2-a]pyridin-3-yl)amino]benzoate (**7k**)

Prepared according to **GP III**. Starting from 2-aminopyridine (0.143 g, 1.50 mmol, 1.00 eq.), (0.149 mL, 0.143 g, 1.65 mmol, 1.10 eq.) butanal, isonitrile **5** (0.296 g 1.65 mmol, 1.10 eq.), and acetic acid (0.171 mL, 0.180 g, 3.00 mmol, 2.00 eq.). The crude mixture was purified by column chromatography ($CHCl_3$/MeOH 1:0 to 99:1 *v*/*v*). Compound **7k** (0.184 g, 0.562 mmol, 37%) was isolated as a brown solid. **R_f** ($CHCl_3$) = 0.18; **mp.** 182 – 184 °C; **^{1}H NMR** (400 MHz, DMSO-d_6) δ = 8.47 (s, 1H), 7.93 (d, *J* = 6.8 Hz, 1H), 7.68 (dd, *J* = 12.3, 1.9 Hz, 1H), 7.58 – 7.46 (m, 2H), 7.29 – 7.18 (m, 1H), 6.91 – 6.81 (m, 1H), 6.19 – 6.05 (m, 1H), 3.78 (s, 3H), 2.57 – 2.51 (m, 2H), 1.66 (sext, *J* = 7.4 Hz, 2H), 0.86 (t, *J* = 7.4 Hz, 3H); **^{13}C NMR** (101 MHz, DMSO-d_6) δ = 165.3, 150.0 (d, *J* = 241.1 Hz), 141.7 (d, *J* = 12.1 Hz), 139.1 (d, *J* = 11.6 Hz), 127.1, 124.2, 122.8, 119.2 (d, *J* = 6.1 Hz), 116.7, 116.1, 115.9, 112.6 (d, *J* = 3.7 Hz), 111.8, 51.8, 28.7, 21.7, 14.0; **^{19}F NMR** (377 MHz, DMSO-d_6) δ = -133.1 (t, *J* = 12.4 Hz); **HRMS-ESI** (*m*/*z*): $[M+H]^+$ calcd for $C_{18}H_{18}FN_3O_2$: 328.1461, found: 328.1459.

Methyl-3-methyl-4-[(2-propylimidazo[1,2-a]pyridin-3-yl)amino]benzoate (**7l**)

2-Aminopyridine (94.0 mg, 1.00 mmol, 1.00 eq.) was dissolved in 3 mL MeOH/CH_2Cl_2 (1/1, *v*/*v*). butanal (91.0 µL, 79.3 mg, 1.10 mmol, 1.10 eq.), isonitrile **6** (0.175 g, 1.00 mmol, 1.00 eq.) and scandium(III)triflate (24.6 mg, 50.0 µmol, 5 mol-%) were added and stirred for three days at room temperature. The solvent was removed under reduced pressure and the crude mixture purified by column chromatography (CyH/EE 1:1 to 1:4 *v*/*v*). Compound **7l** (0.200 g, 0.618 mmol, 62%) was isolated as a white solid. $\mathbf{R_f}$ (CyH/EE 1:2, *v*/*v*) = 0.20; **mp.** 204 – 206 °C; **^{1}H NMR** (600 MHz, $CDCl_3$) δ = 7.90 – 7.83 (m, 1H), 7.71 (dt, *J* = 6.7, 1.2 Hz, 1H), 7.65 (dd, *J* = 8.5, 2.0 Hz, 1H), 7.59 (dt, *J* = 9.1, 1.1 Hz, 1H), 7.20 (ddd, *J* = 9.1, 6.7, 1.3 Hz, 1H), 6.76 (td, *J* = 6.7, 1.2 Hz, 1H), 6.05 (d, *J* = 8.5 Hz, 1H), 5.61 (s, 1H), 3.84 (s, 3H), 2.66 (t, *J* = 7.6 Hz, 2H), 2.43 (s, 3H), 1.75 (h, *J* = 7.4 Hz, 2H), 0.92 (t, *J* = 7.4 Hz, 3H); **^{13}C NMR** (151 MHz, $CDCl_3$) δ = 167.2, 147.6, 143.2, 142.8, 132.6, 129.7, 124.7, 122.3, 121.5, 121.1, 117.5, 117.4, 112.2, 111.0, 51.9, 29.3, 22.5, 17.5, 14.3; **LRMS-ESI** (*m*/*z*): $[M+H]^+$ calcd for $C_{19}H_{21}N_3O_2$: 324.2, found: 324.2.

Methyl 3-fluoro-4-[(2-methylimidazo[1,2-a]pyridin-3-yl)amino]benzoate (**7m**)

Prepared according to **GP III**. Starting from 2-aminopyridine (0.181 g, 1.81 mmol, 1.00 eq.), acetaldehyde (5 M in THF, 0.400 mL, 88.1 mg, 2.00 mmol, 1.10 eq.), isonitrile **5** (0.353 g, 2.00 mmol, 1.10 eq.), and acetic acid (0.207 mL, 0.217 g, 3.62 mmol, 2.00 eq.). The crude mixture was purified by column chromatography (CyH/EE 1:3 to 1:19 *v*/*v*). Compound **7m** (0.144 g, 0.481 mmol, 27%) was isolated as a brown solid. $\mathbf{R_f}$ (CyH/EE 1/3) = 0.10; **mp.** ~147 °C (decomposition); **^{1}H NMR** (600 MHz, DMSO-d_6) δ = 8.46 (d, *J* = 2.2 Hz, 1H), 7.95 (dt, *J* = 6.8, 1.2 Hz, 1H), 7.68 (dd, *J* = 12.3, 1.9 Hz, 1H), 7.54 (dd, *J* = 8.5, 1.9 Hz, 1H), 7.50 (dt, *J* = 9.0, 1.1 Hz, 1H), 7.24 (ddd, *J* = 9.1, 6.7, 1.3 Hz, 1H), 6.86 (td, *J* = 6.7, 1.2 Hz, 1H), 6.16 (t, *J* = 8.6 Hz, 1H), 3.78 (s, 3H), 2.22 (s, 3H); **^{13}C NMR** (151 MHz, DMSO-d_6) δ = 165.3 (d, *J* = 2.7 Hz), 150.0 (d, *J* = 241.0 Hz), 141.6, 138.9 (d, *J* = 11.5 Hz), 137.5, 127.1 (d, *J* = 2.5 Hz), 124.2, 122.8, 119.2 (d, *J* = 6.1 Hz), 116.9, 116.5, 116.0 (d, *J* = 19.3 Hz), 112.6 (d, *J* = 3.6 Hz), 111.7, 51.8, 12.7; **^{19}F NMR** (565 MHz, DMSO-d_6) δ = -133.9 – -134.0 (m); **LRMS-ESI** (*m*/*z*): $[M+H]^+$ calcd for $C_{16}H_{14}FN_3O_2$: 300.1, found: 300.1.

N-Hydroxy-4-[(2-methylimidazo[1,2-a]pyridin-3-yl)amino]benzamide trifluoroacetate (**8a**)

Prepared according to **GP IV.** Starting from (0.100 g, 0.355 mmol, 1.00 eq.) ester **7a**, hydroxyl amine (50% in H_2O, 0.680 mL, 0.336 g, 10.7 mmol, 30.0 eq.), and NaOH (0.140 g, 3.55 mmol, 10.0 eq.). The formed participate was further purified via preparative HPLC. Compound **8a** (29.4 mg, 74.2 µmol, 21%) was isolated as a white lyophilizate. **HPLC**: t_R = 10.12 min (96.0% purity); $\mathbf{R_f}$ (CH_2Cl_2/MeOH 9:1, *v*/*v*) = 0.25; **^{1}H NMR** (500 MHz, DMSO-d_6) δ = 10.96 (s, 1H), 8.66 (s, 1H), 8.34 (dt, *J* = 6.8, 1.1 Hz, 1H), 7.98 (dt, *J* = 9.0, 1.2 Hz, 1H), 7.92 (ddd, *J* = 9.0, 6.9, 1.2 Hz, 1H), 7.64 – 7.60 (m, 2H), 7.43 (td, *J* = 6.9, 1.2 Hz, 1H), 6.73 – 6.66 (m, 2H), 2.37 (s, 3H); **^{13}C**

NMR (126 MHz, DMSO-d_6) δ 164.1, 158.2 (q, J = 32.2 Hz), 147.3, 137.2, 132.6, 128.6, 128.5, 124.8, 123.7, 120.6, 116.8 (q, J = 297.2 Hz), 116.7, 112.9, 112.4, 9.4; **HRMS-ESI** (m/z): $[M+H]^+$ calcd for $C_{15}H_{14}N_4O_2$: 283.1195, found: 283.1187.

4-[(2-Ethylimidazo[1,2-a]pyridin-3-yl)amino]-*N*-hydroxybenzamide (**8b**)

Prepared according to **GP IV.** Starting from ester **7b** (80.0 mg, 0.271 mmol, 1.00 eq.), hydroxyl amine (50% in H_2O, 0.540 mL 0.268 g, 8.13 mmol, 30.0 eq.), and NaOH (0.109 g, 2.72 mmol, 10.0 eq.). Compound **8b** (52.8 mg, 0.178 mmol, 66%) was isolated as a white solid. **HPLC**: t_R = 10.20 min (98.5% purity); **R_f** (CH_2Cl_2/MeOH 9:1, v/v) = 0.30; **mp.** 173 °C – 175 °C; **^{1}H NMR** (300 MHz, DMSO-d_6) δ = 10.87 (s, 1H), 8.81 (s, 1H), 8.24 (s, 1H), 7.90 – 7.81 (m, 1H), 7.57 (d, J = 8.4 Hz, 2H), 7.51 (d, J = 9.0 Hz, 1H), 7.27 – 7.16 (m, 1H), 6.91 – 6.80 (m, 1H), 6.44 (d, J = 8.4 Hz, 2H), 2.59 (q, J = 7.5 Hz, 2H), 1.19 (t, J = 7.5 Hz, 3H); **^{13}C NMR** (101 MHz, DMSO-d_6) δ = 164.5, 149.1, 142.5, 141.5, 128.6, 123.9, 122.7, 122.4, 117.7, 116.7, 112.0, 111.7, 20.1, 13.6; **HRMS-ESI** (m/z): $[M+H]^+$ calcd for $C_{16}H_{16}N_4O_2$: 297.1362, found: 297.1352.

Methyl 4-[(2-isobutylimidazo[1,2-a]pyridin-3-yl)amino]benzoate (**8c**)

Prepared according to **GP IV.** Starting from ester **7c** (80.0 mg, 0.247 mmol, 1.00 eq.), hydroxyl amine (50% in H_2O, 0.492 mL, 0.245 g, 7.41 mmol, 30.0 eq.), and NaOH (98.8 mg, 2.47 mmol, 10.0 eq.). Compound **8c** (64.8 mg, 0.200 mmol, 81%) was isolated as a white solid. **HPLC**: t_R = 10.66 min (96.6% purity); **R_f** (CH_2Cl_2/MeOH 9:1, v/v) = 0.46; **mp.** 171 °C – 173 °C; **^{1}H NMR** (300 MHz, DMSO-d_6) δ = 10.88 (s, 1H), 8.82 (s, 1H), 8.27 (s, 1H), 7.81 (d, J = 6.7 Hz, 1H), 7.56 (d, J = 8.4 Hz, 2H), 7.53 – 7.47 (m, 1H), 7.28 – 7.14 (m, 1H), 6.93 – 6.75 (m, 1H), 6.43 (d, J = 8.3 Hz, 2H), 2.46 (d, J = 7.9 Hz, 2H), 2.14 – 1.98 (m, 1H), 0.85 (d, J = 6.6 Hz, 6H); **^{13}C NMR** (101 MHz, DMSO-d_6) δ = 164.5, 148.9, 141.5, 140.7, 128.6, 123.9, 122.7, 122.3, 118.7, 116.7, 112.1, 111.7, 35.9, 27.8, 22.6; **HRMS-ESI** (m/z): $[M+H]^+$ calcd for $C_{18}H_{20}N_4O_2$: 325.1665, found: 325.1665.

4-[(2-Cyclopropylimidazo[1,2-a]pyridin-3-yl)amino]-*N*-hydroxybenzamide (**8d**)

Prepared according to **GP IV.** Starting from ester **7d** (67.3 mg, 0.220 mmol, 1.00 eq.), hydroxyl amine (50% in H_2O, 0.438 mL, 0.217 g, 6.60 mmol, 30.0 eq.), and NaOH (88.0 mg, 2.20 mmol, 10.0 eq.). Compound **8d** (47.0 mg, 0.132 mmol, 60%) was isolated as a yellow solid. **HPLC**: t_R = 10.32 min (99.0% purity); **R_f** (CH_2Cl_2/MeOH 9:1, v/v) = 0.28; **mp.** 179 – 181 °C; **^{1}H NMR** (400 MHz, DMSO-d_6) δ = 10.75 (s, 1H), 9.02 (s, 0H), 8.35 (s, 1H), 7.84 (dd, J = 6.7, 1.3 Hz, 1H), 7.59 (d, J = 8.3 Hz, 2H), 7.45 (dd, J = 9.0, 1.2 Hz, 1H), 7.19 (ddd, J = 8.7, 6.8, 1.4 Hz, 1H), 6.83 (td, J = 6.8, 1.2 Hz, 1H), 6.53 – 6.44 (m, 2H), 1.88 (tt, J = 8.2, 5.0 Hz, 1H), 0.97 –

0.80 (m, 4H); **^{13}C NMR** (101 MHz, DMSO-d_6) δ = 164.5, 149.1, 142.2, 141.5, 128.6, 123.9, 122.4, 122.4, 118.0, 116.4, 112.1, 111.6, 8.1, 7.9; **HRMS-ESI** (*m*/*z*): $[M+H]^+$ calcd for $C_{17}H_{16}N_4O_2$: 309.1352, found: 309.1347.

4-[(2-Butylimidazo[1,2-a]pyridin-3-yl)amino]-*N*-hydroxybenzamide (**8e**)

Prepared according to **GP IV.** Starting from ester **7e** (69.6 mg, 0.215 mmol, 1.00 eq.), hydroxyl amine (50% in H_2O, 0.428 mL, 0.214 g, 6.45 mmol, 30.0 eq.), and NaOH (86.0 mg, 2.15 mmol, 10.0 eq.). Compound **8e** (63.6 mg 0.196 mmol, 91%) was isolated as a white solid. **HPLC**: t_R = 10.71 min (96.8% purity); **R_f** (CH_2Cl_2/MeOH 9:1, *v*/*v*) = 0.48; **mp.** 155 °C – 157 °C; **^{1}H NMR** (400 MHz, DMSO-d_6) δ = 10.90 (s, 1H), 8.82 (s, 1H), 8.24 (s, 1H), 7.83 (d, *J* = 6.8 Hz, 1H), 7.57 (d, *J* = 8.4 Hz, 2H), 7.50 (d, *J* = 9.0 Hz, 1H), 7.21 (t, *J* = 7.9 Hz, 1H), 6.85 (t, *J* = 6.7 Hz, 1H), 6.43 (d, *J* = 8.4 Hz, 2H), 2.57 (t, *J* = 7.5 Hz, 2H), 1.62 (p, *J* = 7.5 Hz, 2H), 1.27 (sext, *J* = 7.1 Hz, 2H), 0.82 (t, *J* = 7.4 Hz, 3H); **^{13}C NMR** (101 MHz, DMSO-d_6) δ = 164.4, 149.0, 141.5, 141.4, 128.6, 123.9, 122.7, 122.3, 118.1, 116.7, 112.0, 111.7, 30.7, 26.3, 21.9, 13.7; **HRMS-ESI** (*m*/*z*): $[M+H]^+$ calcd for $C_{18}H_{20}N_4O_2$: 325.1665, found: 325.1667.

N-Hydroxy-4-[(2-pentylimidazo[1,2-a]pyridin-3-yl)amino]benzamide (**8f**)

Prepared according to **GP IV.** Starting from ester **7f** (60.0 mg, 0.177 mmol, 1.00 eq.), hydroxyl amine (50% in H_2O, 0.353 mL, 0.176 g, 5.31 mmol, 30.0 eq.), and NaOH (70.8 mg, 1.77 mmol, 10.0 eq.). Compound **8f** (53.8 mg, 0.159 mmol, 90%) was isolated as a white solid. **HPLC**: t_R = 10.95 min (95.0% purity); **R_f** (CH_2Cl_2/MeOH 9:1, *v*/*v*) = 0.50; **mp.** 155 °C – 157 °C; **^{1}H NMR** (400 MHz, DMSO-d_6) δ = 10.88 (s, 1H), 8.79 (s, 1H), 8.25 (s, 1H), 7.83 (d, *J* = 6.8 Hz, 1H), 7.57 (d, *J* = 8.3 Hz, 2H), 7.50 (d, *J* = 9.1 Hz, 1H), 7.21 (t, *J* = 7.8 Hz, 1H), 6.85 (t, *J* = 6.7 Hz, 1H), 6.43 (d, *J* = 8.2 Hz, 2H), 2.57 (t, *J* = 7.5 Hz, 2H), 1.70 – 1.58 (m, 2H), 1.29 – 1.15 (m, 4H), 0.84 – 0.71 (m, 3H); **^{13}C NMR** (101 MHz, DMSO-d_6) δ = 164.5, 149.1, 141.5, 141.4, 128.6, 123.9, 122.6, 122.3, 118.2, 116.7, 112.0, 111.7, 31.0, 28.2, 26.6, 21.9, 13.8; **HRMS-ESI** (*m*/*z*): $[M+H]^+$ calcd for $C_{19}H_{22}N_4O_2$: 339.1821, found: 339.1826.

N-Hydroxy-4-{[2-(3,3,3-trifluoropropyl)imidazo[1,2-a]pyridin-3-yl]amino}benzamide (**8g**)

Prepared according to **GP IV.** Starting from ester **7g** (82.1 mg, 0.226 mmol, 1.00 eq.), hydroxyl amine (50% in H_2O, 0.438 mL, 0.217 g, 6.60 mmol, 30.0 eq.), and NaOH (90.4 mg 2.26 mmol, 10.0 eq.). Compound **8g** (50.3 mg, 0.138 mmol, 61%) was isolated as a yellow solid. **HPLC**: t_R = 10.66 min (95.4% purity); **R_f** (CH_2Cl_2/MeOH 9:1, *v*/*v*) = 0.30, **mp.** > 148 °C (decomposition); **^{1}H NMR** (300 MHz, DMSO-d_6) δ = 10.91 (s, 1H), 8.83 (s, 1H), 8.31 (s, 1H), 7.88 (d, *J* = 6.7 Hz, 1H), 7.66 – 7.49 (m, 3H), 7.26 (dd, *J* = 9.0, 6.7 Hz, 1H), 6.89 (t, *J* = 6.7 Hz, 1H), 6.48 (d, *J* = 8.3 Hz, 2H), 2.88 – 2.77 (m, 2H), 2.76 – 2.55 (m, 2H); **^{13}C NMR** (101 MHz, DMSO-d_6) δ = 164.5, 148.7,

141.6, 137.9, 128.7, 127.3 (d, *J* = 277.2 Hz), 124.5, 122.9, 122.7, 118.5, 116.8, 112.5 – 111.9 (m), 31.9 (q, *J* = 27.6 Hz), 19.5 (q, *J* = 3.5 Hz); **^{19}F NMR** (282 MHz, DMSO) δ = -65.2 (dd, *J* = 12.6, 9.6 Hz); **HRMS-ESI** (*m*/*z*): $[M+H]^+$ calcd for $C_{17}H_{15}F_3N_4O_2$: 365.1225, found: 365.1236.

N-Hydroxy-4-[(6-methyl-2-propylimidazo[1,2-a]pyridin-3-yl)amino]benzamide (**8h**)

Prepared according to **GP IV.** Starting from ester **7h** (82.5 mg, 0.255 mmol, 1.00 eq.), hydroxyl amine (50% in H_2O, 0.484 mL, 0.240 g, 7.65 mmol, 30.0 eq.), and NaOH (0.102 g, 2.55 mmol, 10.0 eq.). Compound **8h** (75.9 mg, 0.234 mmol, 92%) was isolated as a beige solid. **HPLC**: t_R = 10.74 min (97.4% purity); **R_f** (CH_2Cl_2/MeOH 9:1, *v*/*v*) = 0.24; **mp.** 195 – 197 °C**; ^{1}H NMR** (400 MHz, DMSO-d_6) δ = 10.89 (s, 1H), 8.82 (s, 1H), 8.22 (s, 1H), 7.71 (d, *J* = 6.8 Hz, 1H), 7.56 (d, *J* = 8.4 Hz, 2H), 7.27 (s, 1H), 6.69 (dd, *J* = 6.9, 1.6 Hz, 1H), 6.42 (d, *J* = 8.3 Hz, 2H), 2.56 – 2.51 (m, 2H), 2.33 (s, 3H), 1.64 (p, *J* = 7.4 Hz, 2H), 0.85 (t, *J* = 7.4 Hz, 3H); **^{13}C NMR** (101 MHz, DMSO-d_6) δ = 164.6, 149.2, 141.9, 140.8, 134.4, 128.6, 122.3, 122.0, 117.7, 115.1, 114.1, 112.0, 28.7, 21.9, 20.7, 14.0; **HRMS-ESI** (*m*/*z*): $[M+H]^+$ calcd for $C_{18}H_{20}N_4O_2$: 325.1665, found: 325.1675.

4-[(6-Ethyl-2-propylimidazo[1,2-a]pyridin-3-yl)amino]-*N*-hydroxybenzamide (**8i**)

Prepared according to **GP IV.** Starting from ester **7i** (80.0 mg, 0.237 mmol, 1.00 eq.), hydroxyl amine (50% in H_2O, 0.471 mL, 0.233 g, 7.11 mmol, 30.0 eq.), and NaOH (94.8 mg, 2.37 mmol, 10.0 eq.). Compound **8i** (72.8 mg, 0.215 mmol, 91%) was isolated as a beige solid. **HPLC**: t_R = 10.95 min (96.8% purity); **R_f** (CH_2Cl_2/MeOH 9:1, *v*/*v*) = 0.24; **mp.** 205 – 207 °C; **^{1}H NMR** (400 MHz, DMSO-d_6) δ = 10.88 (s, 1H), 8.82 (s, 1H), 8.21 (s, 1H), 7.73 (d, *J* = 6.9 Hz, 1H), 7.56 (d, *J* = 8.4 Hz, 2H), 7.27 (s, 1H), 6.73 (dd, *J* = 7.0, 1.7 Hz, 1H), 6.43 (d, *J* = 8.3 Hz, 2H), 2.64 (q, *J* = 7.5 Hz, 2H), 2.53 (d, *J* = 7.3 Hz, 2H), 1.64 (h, *J* = 7.4 Hz, 2H), 1.20 (t, *J* = 7.5 Hz, 3H), 0.85 (t, *J* = 7.4 Hz, 3H); **^{13}C NMR** (101 MHz, DMSO-d_6) δ = 164.5, 149.2, 142.0, 140.9, 140.4, 128.6, 122.3, 122.2, 117.7, 113.7, 113.0, 112.0, 28.8, 27.6, 21.9, 14.6, 14.0; **HRMS-ESI** (*m*/*z*): $[M+H]^+$ calcd for $C_{19}H_{22}N_4O_2$: 339.1821, found: 339.1826.

N-Hydroxy-4-[(2-propylimidazo[1,2-a]pyrazin-3-yl)amino]benzamide (**8j**)

Prepared according to **GP IV.** Starting from ester **7j** (0.115 g, 0.371 mmol, 1.00 eq.), hydroxyl amine (50% in H_2O, 0.734 mL, 0.367 g, 11.1 mmol, 30.0 eq.), and NaOH (0.148 mg, 3.71 mmol, 10.0 eq.). Compound **8j** (60.1 mg, 0.193 mmol, 52%) was isolated as a white solid. **HPLC**: t_R = 10.32 min (95.8% purity); **R_f** (CH_2Cl_2/MeOH 9:1, *v*/*v*) = 0.28; **mp.** 193 °C – 195 °C; **^{1}H NMR** (400 MHz, DMSO-d_6) δ = 10.90 (s, 1H), 8.97 (s, 1H), 8.79 (s, 1H), 8.43 (d, *J* = 3.1 Hz, 1H), 7.97 – 7.88 (m, 1H), 7.84 (d, *J* = 4.1 Hz, 1H), 7.64 – 7.51 (m, 2H), 6.51 – 6.41 (m, 2H), 2.65 – 2.58 (m, 2H), 1.76 – 1.63 (m, 2H), 0.91 – 0.82 (m, 3H); **^{13}C NMR** (101 MHz,

DMSO-d_6) δ = 164.4, 148.1, 143.7, 142.1, 137.0, 128.9, 128.6, 122.8, 120.2, 116.1, 112.4, 28.7, 21.6, 13.9; **HRMS-ESI** (*m*/*z*): $[M+H]^+$ calcd for $C_{16}H_{17}N_5O_2$: 312.1460, found: 312.1463.

3-Fluoro-*N*-hydroxy-4-[(2-propylimidazo[1,2-a]pyridin-3-yl)amino]benzamide (**8k**)

Prepared according to **GP IV.** Starting from ester **7k** (80.0 mg, 0.244 mmol, 1.00 eq.), hydroxyl amine (50% in H_2O, 0.484 mL, 0.242 g, 7.32 mmol, 30.0 eq.), and NaOH (98.0 mg, 2.44 mmol, 10.0 eq.). Compound **8k** (61.6 mg, 0.188 mmol, 77%) was isolated as a white solid. **HPLC**: t_R = 10.56 min (97.0% purity); $\mathbf{R_f}$ (CH_2Cl_2/MeOH 9:1, *v*/*v*) = 0.40; **mp.** 189 – 191 °C; **^{1}H NMR** (300 MHz, DMSO-d_6) δ = 11.02 (s, 1H), 8.93 (s, 1H), 8.21 (s, 1H), 7.91 (d, *J* = 6.8 Hz, 1H), 7.59 (d, *J* = 12.7 Hz, 1H), 7.52 (d, *J* = 8.9 Hz, 1H), 7.35 (d, *J* = 8.4 Hz, 1H), 7.23 (t, *J* = 7.8 Hz, 1H), 6.86 (t, *J* = 6.8 Hz, 1H), 6.06 (t, *J* = 8.6 Hz, 1H), 2.59 – 2.53 (m, 2H), 1.66 (q, *J* = 7.4 Hz, 2H), 0.86 (t, *J* = 7.3 Hz, 3H); **^{13}C NMR** (101 MHz, DMSO-d_6) δ = 163.3, 150.1 (d, *J* = 240.3 Hz), 141.7, 141.6, 137.0 (d, *J* = 11.5 Hz), 124.2, 124.1, 122.8, 122.5 (d, *J* = 5.4 Hz), 117.1, 116.6, 114.1 (d, *J* = 19.4 Hz), 112.5 (d, *J* = 3.8 Hz), 111.7, 28.7, 21.7, 14.0; **^{19}F NMR** (282 MHz, DMSO-d_6) δ = -133.4 (t, *J* = 10.7 Hz); **HRMS-ESI** (*m*/*z*): $[M+H]^+$ calcd for $C_{17}H_{17}FN_4O_2$: 329.1414, found: 329.1413.

N-Hydroxy-3-methyl-4-[(2-propylimidazo[1,2-a]pyridin-3-yl)amino]benzamide (**8l**)

Prepared according to **GP IV.** Starting from ester **7l** (0.100 g, 0.309 mmol, 1.00 eq.), hydroxyl amine (50% in H_2O, 0.614 mL, 0.304 g, 9.27 mmol, 30.0 eq.), and NaOH (0.124 g, 3.09 mmol, 10.0 eq.). Compound **8l** (73.7 mg, 0.227 mmol, 73%) was isolated as a white solid. **HPLC**: t_R = 10.41 min (98.6% purity); $\mathbf{R_f}$ (CH_2Cl_2/MeOH 9:1, *v*/*v*) = 0.35; **mp.** > 250 °C (decomposition); **^{1}H NMR** (600 MHz, DMSO-d_6) δ = 10.83 (s, 1H), 8.76 (s, 1H), 7.83 (dt, *J* = 6.8, 1.2 Hz, 1H), 7.57 (d, *J* = 2.1 Hz, 1H), 7.53 – 7.48 (m, 2H), 7.31 (dd, *J* = 8.5, 2.1 Hz, 1H), 7.21 (ddd, *J* = 9.0, 6.6, 1.3 Hz, 1H), 6.83 (td, *J* = 6.7, 1.1 Hz, 1H), 5.82 (d, *J* = 8.4 Hz, 1H), 2.55 (t, *J* = 7.5 Hz, 2H), 2.37 (s, 3H), 1.67 (h, *J* = 7.4 Hz, 2H), 0.87 (t, *J* = 7.4 Hz, 3H); **^{13}C NMR** (151 MHz, DMSO-d_6) δ = 165.1, 147.4, 142.1, 142.0, 130.1, 126.5, 124.3, 123.2, 122.7, 122.5, 118.9, 117.1, 112.0, 110.5, 29.3, 22.2, 18.3, 14.5; **HRMS-ESI** (*m*/*z*): $[M+H]^+$ calcd for $C_{18}H_{20}N_4O_2$: 325.1665, found: 325.1660.

3-Fluoro-*N*-hydroxy-4-[(2-methylimidazo[1,2-a]pyridin-3-yl)amino]benzamide (**8m**)

Prepared according to **GP IV.** Starting from ester **7m** (80.0 mg, 0.267 mmol, 1.00 eq.), hydroxyl amine (50% in H_2O, 0.644 mL, 0.251 g, 8.01 mmol, 30.0 eq.), and NaOH (0.107 g, 2.67 mmol, 10.0 eq.). Compound **8m** (48.0 mg, 0.160 mmol, 60%) was isolated as a white solid. **HPLC**: t_R = 10.19 min (96.1% purity); $\mathbf{R_f}$ (CH_2Cl_2/MeOH 9:1, *v*/*v*) = 0.30; **mp.** ~145 °C (decomposition); **^{1}H NMR** (600 MHz, DMSO-d_6) δ = 11.00 (s, 1H), 8.92 (s, 1H), 8.20 (d, *J* = 2.2 Hz, 1H), 7.93 (dt, *J* = 6.8, 1.2 Hz, 1H), 7.59 (dd, *J* = 12.6, 1.9 Hz, 1H), 7.49 (dt,

J = 9.1, 1.2 Hz, 1H), 7.36 (dd, *J* = 8.4, 1.9 Hz, 1H), 7.23 (ddd, *J* = 9.0, 6.7, 1.3 Hz, 1H), 6.86 (td, *J* = 6.7, 1.2 Hz, 1H), 6.08 (t, *J* = 8.6 Hz, 1H), 2.22 (s, 3H); **^{13}C NMR** (151 MHz, DMSO-d_6) δ = 163.2, 150.1 (d, *J* = 240.2 Hz), 141.6, 137.5, 136.8 (d, *J* = 11.6 Hz), 124.2, 124.1, 122.8, 122.6 (d, *J* = 5.4 Hz), 117.4, 116.4, 114.0 (d, *J* = 19.4 Hz), 112.4 (d, *J* = 3.5 Hz), 111.7, 12.7; **^{19}F NMR** (565 MHz, DMSO-d_6) δ = -133.4 (t, *J* = 10.8 Hz); **HRMS-ESI** (*m*/*z*): $[M+H]^+$ calcd for $C_{15}H_{13}FN_4O_2$: 301.1101, found: 301.1097.

4.3 HDAC enzyme inhibition assay

In vitro inhibitory activities against HDAC1−3 and HDAC6 were measured using a previously published protocol.[50] In short, 3-fold serial dilutions of test compounds and controls were prepared in assay buffer (50 mM Tris-HCl (pH 8.0), 137 mM NaCl, 2.7 mM KCl, 1.0 mM $MgCl_2 \cdot 6\ H_2O$, and 0.1 mg/mL BSA). These serial dilutions (5.0 µL) were transferred into 96-well microplates (OptiPlate-96 F, black, PerkinElmer). 35 µL of the fluorogenic substrate ZMAL (Z-Lys(Ac)-AMC[40]; 21.43 µM in assay buffer) and 10 µL of human recombinant HDAC enzyme solution (HDAC1 - BPS Bioscience, Catalog# 50051; HDAC2 - BPS Bioscience, Catalog# 50052; HDAC3/NcoR2 - BPS Bioscience, Catalog# 50003; HDAC6 - BPS Bioscience, Catalog# 50006) were added. The total assay volume of 50 µL (max. 1% DMSO) was incubated at 37 °C for 90 min. Subsequently, 50 µL trypsin solution (0.4 mg/mL trypsin in buffer: 50 mM Tris-HCl (pH 8.0), 100 mM NaCl) was added, followed by 30 min of incubation at 37 °C. Fluorescence (excitation, 355 nm; emission, 460 nm) was measured using a FLUOstar OPTIMA microplate reader (BMG LABTECH). All compounds were tested in duplicates. Reported mean IC_{50}-values, including standard deviation, were calculated from at least two independent experiments.

In vitro inhibitory activity against HDAC10 was performed by *Reaction Biology*. In short, 10 µL of reaction buffer (20 mM Na_2HPO_4 (pH 8.0), 100 mM NaCl, 0.25 mM EDTA, 10 mM Mesna, 0.01% Brij35, 1% DMSO) and/or 10 µL enzyme solution (human full-length HDAC10 (aa2-669end, Accession # NM_032019.5), N-terminal GST-TEV-tag, expressed in Sf9 insect cells) was delivered into wells of 3573 Corning Black react plates. Subsequently, compound dilutions (in 100% DMSO) were delivered into the enzyme mixture and pre-incubated for 20 min. Next, 10 µL of substrate mixture (Ac-spermidine-AMC) was delivered to all reaction wells and incubated for 1 h at 30 °C. The reaction was stopped by the addition of borate buffer (pH 9.5) and NDA (167 µM final). Results was determined by endpoint measurement (Ex/Em=355/460 nm)

4.4 Cell biological evaluation

4.4.1 THP-1 macrophages and J774A.1 macrophages

4.4.1.1 Cell culture

Human THP-1 cells (ACC 16, DSMZ-German Collection of Microorganisms and Cell Cultures GmbH, Braunschweig, Germany) were used from passages 10 to 25 and cultured in RPMI 1640 (2653669, Thermo Fisher Scientific, Darmstadt, Germany), supplemented with 100 U/ml penicillin, 100 µg/ml streptomycin (P4333, Sigma-Aldrich, Taufkirchen, Germany) and 10% heat-inactivated fetal bovine serum (FBS; S0615, Sigma-Aldrich). For differentiation of THP-1 monocytes into THP-1 macrophages, cells were seeded into 24-well plates at a density of 4 x 10^5 cells/well in growth medium. Phorbol 12-myristate 13-acetate (P1585, Sigma-Aldrich) as added to the completed RPMI 1640 medium (25 ng/ml). After 48 h, adherent cells were washed with PBS (phosphate buffered saline; P04-53500, Pan-Biotech, Aidenbach, Germany) and incubated with PMA-free RPMI 1640 for 24 h. Mouse J774A.1 macrophages (CLS Cell Lines Service GMbH, Eppelheim, Germany) were used from passages 39 to 60 and cultured in DMEM (P04-03596, Pan-Biotech) containing 10% heat-inactivated FBS (S0615, Sigma-Aldrich) and 1% L-glutamine. 2 x 10^5 cells/well were seeded into 24 well-plates and rested 24 h before stimulation. Cells were maintained at 37 °C in a humidified atmosphere of 5% CO_2 and 95% air and regularly tested negative for mycoplasma contamination (VenorGeM Classic Mycoplasma PCR detection kit, 11-8100, Minerva Biolabs, Berlin, Germany).

4.4.1.2 Cell stimulation

For inflammasome activation studies, THP-1 macrophages were primed with 100 ng/ml LPS (LPS EB ultrapure, from *Escherchia coli* O111:B4, InvivoGen, Toulouse France) for 3 h. Afterwards, cells were incubated with different concentrations of tubastatin A (S804906, Selleckchem, Houston, Texas, USA), MAIP-032, **8k** and **8m** for 1 h and then stimulated with 5 mM ATP (adenosine 5´-triphosphate, NU-1010-100G, Jena Bioscience, Jena, Germany) or 10 µM nigericin (4312/10, Tocris Bioscience, Bristol, United Kingdom) for 3 h. For J774A.1 macrophages, cells were stimulated for 4.5 h with 1 µg/ml LPS, followed by incubation with tubastatin A or **8k**. Afterwards, cells were stimulated with 2 mM ATP for 1 h or 10 µM nigericin for 3 h. For inflammasome priming studies, THP-1 macrophages were preincubated 24 h with tubastatin A, **MAIP-032**, **8k** and **8m**. Subsequently, medium was removed, and cells were stimulated with 100 ng/ml LPS for 3 h. The pan-HDAC inhibitor vorinostat (10 µM, synthesized according to literature[51]), NLRP3 inhibitor MCC950 (10 µM, 5479, Tocris Bioscience) and DMSO (Dimethylsulfoxide, RNBL6559, Sigma-Aldrich) were used as controls.

4.4.1.3 ELISA

Supernatants were collected and analyzed for human TNF (355053-003, Thermo Fisher Scientific), human IL-1β (316234-006, Thermo Fisher Scientific) and mouse IL-1β (P329282, DuoSet; R&D Systems) secretion following the manufacturer's instructions.

4.4.1.4 Western blotting

Western blot analysis was performed as previously described by us.[49] Membranes were incubated overnight at 4°C with anti-acetyl-histone H3 (1:20,000) (06-599, Merck KGaA, Darmstadt, Germany) antibody and afterwards probed with anti-rabbit HRP-conjugated antibody (1:2000) (7074, Cell Signaling Technology, Leiden, The Netherlands) for 1 h and visualized by ECL solution (Clarity Max Western ECL Substrate; 1705062; Bio-Rad, Feldkirchen, Germany) and ChemiDoc imaging system (Bio-Rad). Protein expression was normalized to total protein amount and analyzed using Image Lab 6.1 (Bio-Rad).

4.4.1.5 RNA isolation, cDNA synthesis and qPCR

Total RNA isolation, cDNA synthesis and quantitative real-time RT-PCR (qRT-PCR) were performed as described previously.[49,52,53] Primers (synthesized by Eurofins, Ebersberg, Germany) with the following sequences were used: *GAPDH*, 5'-CTCTCTGCTCCTCCTGTTCGAC-3' and 5'-TGAGCGATGTGGCTCGGCT-3'; IL1B, 5'-TGGAGCAACAAGTGGTGT-3' and 5'-TTGGGATCTACACTCTCCAGC-3'. Fold difference in gene expression was normalized to the housekeeping gene GAPDH showing the most constant expression levels.

4.4.1.6 Cell viability assays

Cell viability was determined using MTT and LDH assay as described.[49] Absorbance was measured at 492 nm using a microplate reader (Mitras^2 LB 943, Berthold Technologies GmbH & Co. KG, Bad Wildbad, Germany).

4.4.1.7 Statistical analysis

Unless otherwise specified, all experiments were performed at least three times. TNF-ELISA and mRNA experiments were performed in four to six independent experiments with duplicates. Significant differences were assessed by one sample t test against 100%. Data are expressed as means + SEM considered significant at *P ≤ 0.05, **P ≤ 0.01, ***P ≤ 0.001, ****P ≤ 0.0001. Extra sum-of-squares F test was used to evaluate whether inhibitory concentration-response curves were best represented by a monophasic or biphasic model. The monophasic model was preferred unless the extra sum-of-squares F test had a value $P < 0.05$. All IC_{50} values were fitted using a monophasic model with variable slope (four parameters). The parameters are presented as mean with 95% confidence interval. Statistical evaluation was performed using GraphPad Prism 9 (GraphPad software, San Diego, USA).

4.4.2 U-87 MG glioblastoma cell line

4.4.2.1 Cell line and cell culture

The human glioblastoma cell line U-87 MG was cultivated in DMEM medium supplemented with 100 U/mL penicillin, 100 U/mL streptomycin, 2 mM L-glutamine and 10% fetal bovine serum in at a humidified atmosphere at 37 °C containing 5% CO_2. Mycoplasma contamination was routinely excluded by PCR.

4.4.2.2 Cell viability assay

MTT (3-(4,5-dimethylthiazol-2-yl)-2,5-diphenyltetrazolium bromide; Catalog# A2231; *BioChemica*, Applichem GmbH, Darmstadt, Germany) was employed to measure cell viability. A total of 6,000 U-87 MG cells were seeded in duplicates in 96-well plates (*Starlab GmbH*, Hamburg, Germany) with each well containing 90 µL of volume. These cells were subsequently stimulated with dilution series of different compounds. Following an incubation period of 72 hours, 20 µL of freshly prepared MTT solution (5 mg/mL) was added for 1 hour at 37 °C and 5% CO_2. After removing the supernatant, the formazan dye was solubilized in 200 µL DMSO (*Sigma-Aldrich*, Steinheim, Germany). The absorbance of the plates was then measured at 570 nm using a Multiskan microplate photometer (*Thermo Fisher Scientific*, Waltham, MA, USA) with background subtraction at 690 nm. The acquired data was normalized to DPBS, considering 100% viability, and analyzed using nonlinear regression to determine IC_{50} values (*GraphPad* Prism 8, San Diego, CA, USA).

4.4.2.3 Immunoblot analysis

U-87 MG cells were seeded to cell culture flasks and allowed to adhere for 24 hours. After that cells were treated with a concentration of 10 µM of HDACi or vehicle (DMSO) for additional 24 hours. For cell lysis the cells were initially washed with PBS and detached using a scraper. The cells were then centrifuged at 1,200 rpm for 4 minutes at 4 °C, followed by two additional washing steps. Afterwards, the cell pellet was resuspended in 100 µL of freshly prepared lysis buffer and incubated on ice for 30 minutes with vortexing every 10 minutes. The lysis buffer consisted of Invitrogen cell extraction buffer (10 mM Tris, pH 7.4, 100 mM NaCl, 1 mM EDTA, 1 mM EGTA, 1 mM NaF, 20 mM $Na_4P_2O_7$, 2 mM Na_3VO_4, 1% Triton™ ×-100, 10% glycerol, 0.1% SDS, 0.5% deoxycholate; Catalog# FNN0011, *Thermo Fisher Scientific Inc*., Waltham, MA, USA), supplemented with 0.1 mM PMSF (Catalog# 10837091001, *Sigma-Aldrich*, St. Louis, MO, USA) and Halt™ Protease Inhibitor (100x) (Catalog# 78429, *Life Technologies GmbH* Carlsbad, CA, USA). Finally, the samples were centrifuged at 14,000 rpm and 4 °C for 30 minutes and the supernatant was collected. Protein quantification was performed by using BCA protein assay reagents (Catalog# 23225, *Thermo Fisher Scientific Inc*., Waltham, MA, USA). Lysates were mixed with Laemmli sample buffer 2x concentrate (Catalog# S3401-10VL, *Sigma-Aldrich*, St. Louis, MO, USA) to a protein concentration of 1.25 µg/µL and denatured at 95 °C for 5 minutes. Subsequently, SDS-PAGE was performed with 12% Mini-PROTEAN TGX stain-free gels (Catalog# 4568045, *Bio-Rad*, Hercules, CA, USA) at 200 V for 45 minutes. Proteins were then transferred to a Trans-Blot Turbo®-PVDF membrane (Catalog# 1704156, *Bio-Rad*, Hercules, CA, USA) with the Trans-Blot Turbo Transfer System (Catalog# 1704150, *Bio-Rad*, Hercules, CA, USA) at 1.0 A for 30 minutes. The membrane was blocked with a solution of 5% milk powder in TBST (Tris-buffered saline-Tween 20 0.2%) for 60 minutes at room temperature. After three washing cycles for 10 minutes

with TBST, the membrane was incubated with the respective antibody at room temperature for 60 minutes and 4 °C overnight. For detection of GAPDH and the acetylation levels of Histone H3 and α-Tubulin, antibodies specific for GAPDH (Catalog# T0004, *Affinity Biosciences*, Cincinnati, OH, USA; 1:20,000 dilution), acetyl-Histone H3 (K9/K14) (Catalog# 9677S, *Cell Signaling Technology*, Denver, MA, USA; 1:1000 dilution) and acetyl-α-Tubulin (Lys40) (Catalog#5335, *Cell Signaling Technology*, Denver, MA, USA: 1:1000 dilution) were used as primary antibodies. The membrane was rinsed again three times before applying the secondary antibody for 1.5 hours at room temperature. As secondary antibody HRP-conjugated anti-mouse IgGκ binding protein (Catalog# sc-516102, *Santa Cruz*, Dallas, TX, USA; 1:10000 dilution) and HRP-conjugated anti-rabbit IgG antibody (Catalog# HAF008, *R&D Systems, Inc.*, Minneapolis, MN, USA; 1:10000 dilution) were employed. After washing off the secondary antibody, protein bands were detected via chemiluminescence using Clarity Western ECL substrate (Catalog# 1705061, *Bio-Rad*, Hercules, CA, USA). Detection and analysis were performed with ChemiDox XRS+ System (Catalog# 1708265, *Bio-Rad*, Hercules, CA, USA) and Image Lab software v. 6.1 (*Bio-Rad*, Hercules, CA, USA).

4.4.2.4 Wound healing assay

In total 3×10^5 U-87 MG cells/well were seeded in a 24-well plate (*Starlab GmbH*, Hamburg, Germany). After 24 hours the cell culture medium was replaced with serum free medium and cells were treated with 10 µM of the respective HDACi. Following a 24-hour preincubation period, the cell monolayer was gently scratched across the centre of each well with a sterile 200 µL pipette tip. Subsequently, cells were carefully washed once with PBS and a fresh serum-free medium containing the same inhibitor was added. The scratched cells were then incubated at 37 °C and 5% CO_2. The process of wound healing was monitored for 48 hours at regular intervals with 10fold magnification with a Axiovert 200 microscope (*Carl Zeiss Microscopy*, Jena, Germany). The acquired images were analyzed with ImageJ (*Tiago Ferreira*, Wayne Rasband), ZEN® 3.0 blue edition (*Carl Zeiss Microscopy*, Oberkochen, Germany) and evaluated with *GraphPad* Prism 8 (San Diego, CA, USA). Wound closure was quantified as relative area (%) compared to initial area. GraphPad Prism Version 8 was used for statistical analysis. One-way ANOVA followed by Dunnett's multiple comparisons test was applied for statistical analysis. ns: not significant; *P ≤ 0.05, **P ≤ 0.01, ***P ≤ 0.001.

*4.4.3 Docking of **8a**, **8f**, and **8k** in zHDAC6 with RosettaLigand*

The crystal structure of the catalytic domain 2 (CD2) of HDAC6 from *danio reriro* (PDB: 6CGP)[37] was obtained from the Protein Data Bank (PDB, www.rcsb.org). All heteroatom records were removed, except for the metal ions (one zinc ion and two potassium ions) and the catalytic water molecule next to the zinc ion. The structure was

optimized to the closest local energy minimum using RosettaRelax with coordinate constraint on the backbone and metal ion restraints.[54] Ligand input files for **8a**, **8f**, and **8k** were created with ChemDraw. An initial 3D conformer with hydrogen atoms was constructed in Chem3D and energetically minimized using the MM2 force field, followed by the production of an ensemble of 1000 low energy conformers with BCL:ConformerGenerator.[55] One conformer was placed in the binding pocket of HDAC6 CD2. A constraint file was constructed using the known distance of the zinc binding of hydroxamic acids.[36] Ligand docking was performed with RosettaLigand (version 3.12) for 5000 models. Those models were clustered according to their similarity in their binding mode. The depicted models are the best scoring models from the cluster with the lowest delta-RMDS values.[56–58]

Acknowledgments

FKH and GW acknowledge partial funding by the Deutsche Forschungsgemeinschaft (DFG, German Research Foundation) – GRK2873 (494832089).

References

(1) Roche, J.; Bertrand, P. Inside HDACs with more selective HDAC inhibitors. *Eur. J. Med. Chem.* **2016**, *121*, 451-483. DOI: 10.1016/j.ejmech.2016.05.047.

(2) Park, S.-Y.; Kim, J.-S. A short guide to histone deacetylases including recent progress on class II enzymes. *EMM* **2020**, *52* (2), 204-212. DOI: 10.1038/s12276-020-0382-4.

(3) Yoshida, M.; Kudo, N.; Kosono, S.; Ito, A. Chemical and structural biology of protein lysine deacetylases. *Proc. Jpn. Acad. Ser. B Phys. Biol. Sci.* **2017**, *93* (5), 297–321. DOI: 10.2183/pjab.93.019.

(4) Jiang, Y.; Liu, J.; Di Chen; Yan, L.; Zheng, W. Sirtuin Inhibition: Strategies, Inhibitors, and Therapeutic Potential. *Trends Pharmacol. Sci.* **2017**, *38* (5), 459–472. DOI: 10.1016/j.tips.2017.01.009.

(5) Wang, P.; Wang, Z.; Liu, J. Role of HDACs in normal and malignant hematopoiesis. *Mol. Cancer* **2020**, *19* (1), 1–27. DOI: 10.1186/s12943-019-1127-7.

(6) Kaluza, D.; Kroll, J.; Gesierich, S.; Yao, T.-P.; Boon, R. A.; Hergenreider, E.; Tjwa, M.; Rössig, L.; Seto, E.; Augustin, H. G.; Zeiher, A. M.; Dimmeler, S.; Urbich, C. Class IIb HDAC6 regulates endothelial cell migration and angiogenesis by deacetylation of cortactin. *EMBO J.* **2011**, *30* (20), 4142-4156. DOI: 10.1038/emboj.2011.298.

(7) Kilgore, M.; Miller, C. A.; Fass, D. M.; Hennig, K. M.; Haggarty, S. J.; Sweatt, J. D.; Rumbaugh, G. Inhibitors of class 1 histone deacetylases reverse contextual memory deficits in a mouse model of Alzheimer's disease. *Neuropsychopharmacology* **2010**, *35* (4), 870-880. DOI: 10.1038/npp.2009.197.

(8) Cao, F.; Zwinderman, M. R. H.; Dekker, F. J. The Process and Strategy for Developing Selective Histone Deacetylase 3 Inhibitors. *Molecules* **2018**, *23* (3), 551. DOI: 10.3390/molecules23030551.

(9) Cappellacci, L.; Perinelli, D. R.; Maggi, F.; Grifantini, M.; Petrelli, R. Recent Progress in Histone Deacetylase Inhibitors as Anticancer Agents. *Curr. Med. Chem.* **2020**, *27* (15), 2449-2493. DOI: 10.2174/0929867325666181016163110.

(10) Ho, T. C. S.; Chan, A. H. Y.; Ganesan, A. Thirty Years of HDAC Inhibitors: 2020 Insight and Hindsight. *J. Med. Chem.* **2020**, *63* (21), 12460–12484. DOI: 10.1021/acs.jmedchem.0c00830.

(11) Ibrahim, N.; Buchbinder, E. I.; Granter, S. R.; Rodig, S. J.; Giobbie-Hurder, A.; Becerra, C.; Tsiaras, A.; Gjini, E.; Fisher, D. E.; Hodi, F. S. A phase I trial of panobinostat (LBH589) in patients with metastatic melanoma. *Cancer Med.* **2016**, *5* (11), 3041-3050. DOI: 10.1002/cam4.862.

(12) San-Miguel, J. F.; Hungria, V. T. M.; Yoon, S.-S.; Beksac, M.; Dimopoulos, M. A.; Elghandour, A.; Jedrzejczak, W. W.; Günther, A.; Nakorn, T. N.; Siritanaratkul, N.; Corradini, P.; Chuncharunee, S.; Lee, J.-J.; Schlossman, R. L.; Shelekhova, T.; Yong, K.; Tan, D.; Numbenjapon, T.; Cavenagh, J. D.; Hou, J.; LeBlanc, R.; Nahi, H.; Qiu, L.; Salwender, H.; Pulini, S.; Moreau, P.; Warzocha, K.; White, D.; Bladé, J.; Chen, W.; La Rubia, J. de; Gimsing, P.; Lonial, S.; Kaufman, J. L.; Ocio, E. M.; Veskovski, L.; Sohn, S. K.; Wang, M.-C.; Lee, J. H.; Einsele, H.; Sopala, M.; Corrado, C.; Bengoudifa, B.-R.; Binlich, F.; Richardson, P. G. Panobinostat plus bortezomib and dexamethasone versus placebo plus bortezomib and dexamethasone in patients with relapsed or relapsed and refractory multiple myeloma: a multicentre, randomised, double-blind phase 3 trial. *Lancet Oncol.* **2014**, *15* (11), 1195-1206. DOI: 10.1016/S1470-2045(14)70440-1.

(13) Ning, Z. Why ACE—overview of the development of the subtype-selective histone deacetylase inhibitor chidamide in hormone receptor positive advanced breast cancer. *Transl. Breast Cancer Res.* **2020**, *1*, 1-10. DOI: 10.21037/tbcr.2020.03.06.

(14) Lee, H.-Z.; Kwitkowski, V. E.; Del Valle, P. L.; Ricci, M. S.; Saber, H.; Habtemariam, B. A.; Bullock, J.; Bloomquist, E.; Li Shen, Y.; Chen, X.-H.; Brown, J.; Mehrotra, N.; Dorff, S.; Charlab, R.; Kane, R. C.; Kaminskas, E.; Justice, R.; Farrell, A. T.; Pazdur, R. FDA Approval: Belinostat for the Treatment of Patients with Relapsed or Refractory Peripheral T-cell Lymphoma. *Clin. Cancer Res.* **2015**, *21* (12), 2666–2670. DOI: 10.1158/1078-0432.CCR-14-3119.

(15) Eleutherakis-Papaiakovou, E.; Kanellias, N.; Kastritis, E.; Gavriatopoulou, M.; Terpos, E.; Dimopoulos, M. A. Efficacy of Panobinostat for the Treatment of Multiple Myeloma. *J. Oncol.* **2020**, *2020*, 1-12. DOI: 10.1155/2020/7131802.

(16) Hogg, S. J.; Beavis, P. A.; Dawson, M. A.; Johnstone, R. W. Targeting the epigenetic regulation of antitumour immunity. *Nat. Rev. Drug. Discov.* **2020**, *19* (11), 776-800. DOI: 10.1038/s41573-020-0077-5.

(17) Liu, Y.; Peng, L.; Seto, E.; Huang, S.; Qiu, Y. Modulation of histone deacetylase 6 (HDAC6) nuclear import and tubulin deacetylase activity through acetylation. *JBC* **2012**, *287* (34), 29168-29174. DOI: 10.1074/jbc.M112.371120.

(18) Brindisi, M.; Saraswati, A. P.; Brogi, S.; Gemma, S.; Butini, S.; Campiani, G. Old but Gold: Tracking the New Guise of Histone Deacetylase 6 (HDAC6) Enzyme as a Biomarker and Therapeutic Target in Rare Diseases. *J. Med. Chem.* **2020**, *63* (1), 23-39. DOI: 10.1021/acs.jmedchem.9b00924.

(19) Cook, C.; Carlomagno, Y.; Gendron, T. F.; Dunmore, J.; Scheffel, K.; Stetler, C.; Davis, M.; Dickson, D.; Jarpe, M.; DeTure, M.; Petrucelli, L. Acetylation of the KXGS motifs in tau is a critical determinant in modulation of tau aggregation and clearance. *Hum. Mol. Genet.* **2014**, *23* (1), 104–116. DOI: 10.1093/hmg/ddt402.

(20) Hubbert, C.; Guardiola, A.; Shao, R.; Kawaguchi, Y.; Ito, A.; Nixon, A.; Yoshida, M.; Wang, X.-F.; Yao, T.-P. HDAC6 is a microtubule-associated deacetylase. *Nature* **2002**, *417* (6887), 455-458. DOI: 10.1038/417455a.

(21) Campiani, G.; Cavella, C.; Osko, J. D.; Brindisi, M.; Relitti, N.; Brogi, S.; Saraswati, A. P.; Federico, S.; Chemi, G.; Maramai, S.; Carullo, G.; Jaeger, B.; Carleo, A.; Benedetti, R.; Sarno, F.; Lamponi, S.; Rottoli, P.; Bargagli, E.; Bertucci, C.; Tedesco, D.; Herp, D.; Senger, J.; Ruberti, G.; Saccoccia, F.; Saponara, S.; Gorelli, B.; Valoti, M.; Kennedy, B.; Sundaramurthi, H.; Butini, S.; Jung, M.; Roach, K. M.; Altucci, L.; Bradding, P.; Christianson, D. W.; Gemma, S.; Prasse, A. Harnessing the Role of HDAC6 in Idiopathic Pulmonary Fibrosis: Design, Synthesis, Structural Analysis, and Biological Evaluation of Potent Inhibitors. *J. Med. Chem.* **2021**, *64* (14), 9960-9988. DOI: 10.1021/acs.jmedchem.1c00184.

(22) Depetter, Y.; Geurs, S.; Vreese, R. de; Goethals, S.; Vandoorn, E.; Laevens, A.; Steenbrugge, J.; Meyer, E.; Tullio, P. de; Bracke, M.; D'hooghe, M.; Wever, O. de. Selective pharmacological inhibitors of HDAC6 reveal biochemical activity but functional tolerance in cancer models. *Int. J. Cancer* **2019.** DOI: 10.1002/ijc.32169.

(23) Witt, O.; Deubzer, H. E.; Milde, T.; Oehme, I. HDAC family:What are the cancer relevant targets? *Cancer let.* **2009**, *277* (1), 8–21. DOI: 10.1016/j.canlet.2008.08.016.

(24) Zhang, Y.; Kwon, S.; Yamaguchi, T.; Cubizolles, F.; Rousseaux, S.; Kneissel, M.; Cao, C.; Li, N.; Cheng, H.-L.; Chua, K.; Lombard, D.; Mizeracki, A.; Matthias, G.; Alt, F. W.; Khochbin, S.; Matthias, P. Mice lacking histone deacetylase 6 have hyperacetylated tubulin but are viable and develop normally. *Mol. Cell. Biol.* **2008**, *28* (5), 1688–1701. DOI: 10.1128/MCB.01154-06.

(25) Magupalli, V. G.; Negro, R.; Tian, Y.; Hauenstein, A. V.; Di Caprio, G.; Skillern, W.; Deng, Q.; Orning, P.; Alam, H. B.; Maliga, Z.; Sharif, H.; Hu, J. J.; Evavold, C. L.; Kagan, J. C.; Schmidt, F. I.; Fitzgerald, K. A.; Kirchhausen, T.; Li, Y.; Wu, H. HDAC6 mediates an aggresome-like mechanism for NLRP3 and pyrin inflammasome activation. *Science* **2020**, *369* (6510). DOI: 10.1126/science.aas8995.
(26) Swanson, K. V.; Deng, M.; Ting, J. P.-Y. The NLRP3 inflammasome: molecular activation and regulation to therapeutics. *Nat. Rev. Immonol* **2019**, *19* (8), 477–489. DOI: 10.1038/s41577-019-0165-0.
(27) Dinarello, C. A. Interleukin-1 in the pathogenesis and treatment of inflammatory diseases. *Blood* **2011**, *117* (14), 3720–3732. DOI: 10.1182/blood-2010-07-273417.
(28) Coll, R. C.; Schroder, K.; Pelegrín, P. NLRP3 and pyroptosis blockers for treating inflammatory diseases. *Trends Pharmacol. Sci.* **2022**, *43* (8), 653–668. DOI: 10.1016/j.tips.2022.04.003.
(29) Mangan, M. S. J.; Olhava, E. J.; Roush, W. R.; Seidel, H. M.; Glick, G. D.; Latz, E. Targeting the NLRP3 inflammasome in inflammatory diseases. *Nat. Rev. Drug Discov.* **2018**, *17* (8), 588–606. DOI: 10.1038/nrd.2018.97.
(30) Lambona, C.; Zwergel, C.; Fioravanti, R.; Valente, S.; Mai, A. Histone deacetylase 10: A polyamine deacetylase from the crystal structure to the first inhibitors. *Curr. Opin. Struct. Biol.* **2023**, *82*, 102668. DOI: 10.1016/j.sbi.2023.102668.
(31) Wang, L.; Zheng, S.; Zhang, L.; Xiao, H.; Gan, H.; Chen, H.; Zhai, X.; Liang, P.; Zhao, J.; Li, Y. Histone Deacetylation 10 Alleviates Inflammation After Intracerebral Hemorrhage via the PTPN22/NLRP3 Pathway in Rats. *Neuroscience* **2020**, *432*, 247–259. DOI: 10.1016/j.neuroscience.2020.02.027.
(32) Yang, M.; Qin, Z.; Lin, Y.; Lv, X.; Sun, C.; Cheng, Y.; Xuan, H.; Cui, X.; Ma, W.; Han, L. *HDAC10 negatively regulates NLRP3 inflammasome activation by switching NLRP3 modification from acetylation to ubiquitination*. Preprint from Research Square, 2023; This content is a preprint and has not been peer-reviewed. DOI: 10.21203/rs.3.rs-2792906/v1.
(33) Grozinger, C. M.; Hassig, C. A.; Schreiber, S. L. Three proteins define a class of human histone deacetylases related to yeast Hda1p. *Proc. Natl. Acad. Sci. USA* **1999**, *96* (9), 4868–4873. DOI: 10.1073/pnas.96.9.4868.
(34) Osko, J. D.; Christianson, D. W. Structural Basis of Catalysis and Inhibition of HDAC6 CD1, the Enigmatic Catalytic Domain of Histone Deacetylase 6. *Biochemistry* **2019**, *58* (49), 4912-4924. DOI: 10.1021/acs.biochem.9b00934.
(35) Hai, Y.; Christianson, D. W. Histone deacetylase 6 structure and molecular basis of catalysis and inhibition. *Nature Chem. Bio.* **2016**, *12* (9), 741–747. DOI: 10.1038/nchembio.2134.
(36) Porter, N. J.; Osko, J. D.; Diedrich, D.; Kurz, T.; Hooker, J. M.; Hansen, F. K.; Christianson, D. W. Histone Deacetylase 6-Selective Inhibitors and the Influence of Capping Groups on Hydroxamate-Zinc Denticity. *J. Med.Chem.* **2018**, *61* (17), 8054-8060. DOI: 10.1021/acs.jmedchem.8b01013.
(37) Mackwitz, M. K. W.; Hamacher, A.; Osko, J. D.; Held, J.; Schöler, A.; Christianson, D. W.; Kassack, M. U.; Hansen, F. K. Multicomponent Synthesis and Binding Mode of Imidazo[1,2- a]pyridine-Capped Selective HDAC6 Inhibitors. *Org. Let.* **2018**, *20*, 3255-3258. DOI: 10.1021/acs.orglett.8b01118.
(38) Sandrone, G.; Cukier, C. D.; Zrubek, K.; Marchini, M.; Vergani, B.; Caprini, G.; Fossati, G.; Steinkühler, C.; Stevenazzi, A. Role of Fluorination in the Histone Deacetylase 6 (HDAC6) Selectivity of Benzohydroxamate-Based Inhibitors. *ACS Med. Chem. Lett.* **2021**, *12* (11), 1810–1817. DOI: 10.1021/acsmedchemlett.1c00425.
(39) Groebke, K.; Weber, L.; Mehlin, F. Synthesis of Imidazo[1,2-a] annulated Pyridines, Pyrazines and Pyrimidines by a Novel Three-Component Condensation. *Synlett* **1998**, *1998* (6), 661–663. DOI: 10.1055/s-1998-1721.
(40) Kraft, F. B.; Hanl, M.; Feller, F.; Schäker-Hübner, L.; Hansen, F. K. Photocaged Histone Deacetylase Inhibitors as Prodrugs in Targeted Cancer Therapy. *Pharmaceuticals* **2023**, *16* (3), 356. DOI: 10.3390/ph16030356.
(41) Reßing, N.; Sönnichsen, M.; Osko, J. D.; Schöler, A.; Schliehe-Diecks, J.; Skerhut, A.; Borkhardt, A.; Hauer, J.; Kassack, M. U.; Christianson, D. W.; Bhatia, S.; Hansen, F. K. Multicomponent Synthesis, Binding Mode, and Structure-Activity Relationship of Selective Histone Deacetylase 6 (HDAC6) Inhibitors with Bifurcated Capping Groups. *J. Med. Chem.* **2020**, *63* (18), 10339–10351. DOI: 10.1021/acs.jmedchem.9b01888.
(42) Liu, J.-R.; Yu, C.-W.; Hung, P.-Y.; Hsin, L.-W.; Chern, J.-W. High-selective HDAC6 inhibitor promotes HDAC6 degradation following autophagy modulation and enhanced antitumor immunity in glioblastoma. *Biochem. Pharmacol.* **2019**, *163*, 458-471. DOI: 10.1016/j.bcp.2019.03.023. Published Online: Mar. 15, 2019.
(43) Chang, P.; Li, H.; Hu, H.; Li, Y.; Wang, T. The Role of HDAC6 in Autophagy and NLRP3 Inflammasome. *Front. Immunol.* **2021**, *12*, 763831. DOI: 10.3389/fimmu.2021.763831.
(44) Yue, K.; Sun, S.; Jia, G.; Qin, M.; Hou, X.; Chou, C. J.; Huang, C.; Li, X. First-in-Class Hydrazide-Based HDAC6 Selective Inhibitor with Potent Oral Anti-Inflammatory Activity by Attenuating NLRP3 Inflammasome Activation. *J. Med. Chem.* **2022**, *65* (18), 12140–12162. DOI: 10.1021/acs.jmedchem.2c00853.
(45) Yan, S.; Wei, X.; Jian, W.; Qin, Y.; Liu, J.; Zhu, S.; Jiang, F.; Lou, H.; Zhang, B. Pharmacological Inhibition of HDAC6 Attenuates NLRP3 Inflammatory Response and Protects Dopaminergic Neurons in Experimental Models of Parkinson's Disease. *Front. Aging. Neurosci.* **2020**, *12*, 78–92. DOI: 10.3389/fnagi.2020.00078.
(46) Chen, Q.; Wang, Y.; Jiao, F.; Cao, P.; Shi, C.; Pei, M.; Wang, L.; Gong, Z. HDAC6 inhibitor ACY1215 inhibits the activation of NLRP3 inflammasome in acute liver failure by regulating the ATM/F-actin signalling pathway. *J. cell. Mol. Med.* **2021**, *25* (15), 7218–7228. DOI: 10.1111/jcmm.16751.
(47) Hwang, I.; Lee, E.; Jeon, S.-A.; Yu, J.-W. Histone deacetylase 6 negatively regulates NLRP3 inflammasome activation. *Biochem. Biophys. Res. commun.* **2015**, *467* (4), 973–978. DOI: 10.1016/j.bbrc.2015.10.033.
(48) Bockstiegel, J.; Engelhardt, J.; Weindl, G. P2X7 receptor activation leads to NLRP3-independent IL-1β release by human macrophages. *Cell communication and signaling : CCS* **2023**, *21* (1), 335. DOI: 10.1186/s12964-023-01356-1. Published Online: Nov. 23, 2023.
(49) Bockstiegel, J.; Wurnig, S. L.; Engelhardt, J.; Enns, J.; Hansen, F. K.; Weindl, G. Pharmacological inhibition of HDAC6 suppresses NLRP3 inflammasome-mediated IL-1β release. *Biochem. Pharmacol.* **2023**, *215*, 115693. DOI: 10.1016/j.bcp.2023.115693.
(50) Schäker-Hübner, L.; Warstat, R.; Ahlert, H.; Mishra, P.; Kraft, F. B.; Schliehe-Diecks, J.; Schöler, A.; Borkhardt, A.; Breit, B.; Bhatia, S.; Hügle, M.; Günther, S.; Hansen, F. K. 4-Acyl Pyrrole Capped HDAC Inhibitors: A New Scaffold for Hybrid Inhibitors of BET Proteins and Histone Deacetylases as Antileukemia Drug Leads. *J. Med. Chem.* **2021**, *64* (19), 14620-14646. DOI: 10.1021/acs.jmedchem.1c01119.
(51) Gediya, L. K.; Chopra, P.; Purushottamachar, P.; Maheshwari, N.; Njar, V. C. O. A new simple and high-yield synthesis of suberoylanilide hydroxamic acid and its inhibitory effect alone or in combination with retinoids on proliferation of human prostate cancer cells. *J. Med. Chem.* **2005**, *48* (15), 5047–5051. DOI: 10.1021/jm058214k.
(52) Müller, G.; Lübow, C.; Weindl, G. Lysosomotropic beta blockers induce oxidative stress and IL23A production in Langerhans cells. *Autophagy* **2020**, *16* (8), 1380–1395. DOI: 10.1080/15548627.2019.1686728.

(53) Lübow, C.; Bockstiegel, J.; Weindl, G. Lysosomotropic drugs enhance pro-inflammatory responses to IL-1β in macrophages by inhibiting internalization of the IL-1 receptor. *Biochem. Pharmaco.* **2020**, *175*, 113864. DOI: 10.1016/j.bcp.2020.113864.
(54) Nivón, L. G.; Moretti, R.; Baker, D. A Pareto-optimal refinement method for protein design scaffolds. *PloS one* **2013**, *8* (4), e59004. DOI: 10.1371/journal.pone.0059004.
(55) Kothiwale, S.; Mendenhall, J. L.; Meiler, J. BCL:Conf: small molecule conformational sampling using a knowledge based rotamer library. *Cheminform* **2015**, *7*, 1–15. DOI: 10.1186/s13321-015-0095-1.
(56) DeLuca, S.; Khar, K.; Meiler, J. Fully Flexible Docking of Medium Sized Ligand Libraries with RosettaLigand. *PloS one* **2015**, *10* (7), e0132508. DOI: 10.1371/journal.pone.0132508.
(57) Kaufmann, K. W.; Meiler, J. Using RosettaLigand for small molecule docking into comparative models. *PloS one* **2012**, *7* (12), e50769. DOI: 10.1371/journal.pone.0050769.
(58) Meiler, J.; Baker, D. ROSETTALIGAND: protein-small molecule docking with full side-chain flexibility. *Proteins* **2006**, *65* (3), 538-548. DOI: 10.1002/prot.21086.